High-n Stability of a pressure discontinuity in a three-dimensional plasma

David Barmaz[1]

E-mail: david.barmaz@gmail.com

Supervisors: Pr. Robert L. Dewar[2]**, Dr. Matthew John Hole**[2]**, Dr. Wilfred Anthony Cooper**[1] **and Pr. Minh Quang Tran**[1]

[1] Ecole Polytechnique Fédérale de Lausanne (EPFL), Centre de Recherche en Physique des Plasmas, CH1015 Lausanne, Switzerland
[2] Plasma Research Laboratory, Research School of Physics and Engineering, The Australian University, Canberra 0200, Australia

Abstract. The critical component of a collaborative project [1] between The Australian National University (ANU) and Princeton Plasma Physics Laboratory (PPPL) on constructing 3-D MHD equilibria, in a way fully compatible with the existence of chaotic magnetic fields, is establishing the existence and stability of good magnetic surfaces with irrational rotational transform that can sustain a pressure jump. Physically, these would form electron transport barriers. The existence of surfaces that satisfy force balance is quite well established [2] and numerical implementations have already been done to confirm their existence. However, the question of stability to displacements of the interface still has to be investigated. It is of particular interest to study how high-n MHD stability relates to the chaos theory limitations on existence [2]. In this project we adapt a theory developed by Bernstein *et al* [4] for high-n MHD stability at an interface between a vacuum magnetic field and a field-free plasma to the problem of general fields. We study in particular the stability at the interface in the case close to zero magnetic shear. We found a simple sufficient condition for high-n interface stability to surface displacement: the interface is stable if all points of zero magnetic shear have favorable curvature. We complete the theoretical approach by implementing the results obtained on a test case.

Contents

1. Introduction

The beginning of the 21^{st} century is characterized by a strong increase in world energy consumption, by fear of a new petrol crisis and by a growing preoccupation with human influence on climate. All these elements induce an environment extremely favorable for the development of new renewable energies. There is, in particular, a big hope placed in nuclear fusion. It is expected to become one of the main energy sources in the future.

The principle of the nuclear fusion reactors is to confine a plasma, i.e. a quasineutral ionized gas, and to extract energy out of it. Two main types of machines using toroidal magnetic field were conceived to achieve this objective : tokamaks and stellarators.

A tokamak is a device that uses strong magnetic fields to confine the plasma. It has an axisymmetric toroidal shape, as shown on figure 1. In a tokamak, the magnetic field lines move around the torus in a helical fashion. This helical field is generated by both a toroidal field (produced by electromagnets that surround the torus) and a poloidal field (which results from a toroidal electric current that flows inside the plasma). The plasma injected in such a reactor is generally made of a mix of deuterium and tritium ions. The critical part of the concept is to manage to gain energy by making these nuclei fuse.

The second most important type of fusion reactor, the stellarator, also uses strong magnetic fields to confine the plasma. But this device differs from the tokamak in the fact that there is no current driven through the plasma itself. Furthermore, the stellarators are not azimuthally symmetric. As can be seen in figure 4, their magnetic coils must have a more complex shape than that of the tokamak, as they need to make the field lines helical.

A lot of interest and a lot of hope are placed in the new experimental devices, such as the tokamak ITER (International Thermonuclear Experimental Reactor), being constructed at the moment in France. But research still has a long way to go before being able to construct a reactor that can produce electric energy at a competitive price.

In parallel to the experimental research, theoreticians are very active to try to understand the complex physics of plasma confinement. An important fraction of the efforts of the theoreticians is, at the moment, concentrated on the study of magnetohydrodynamic stability. Magnetohydrodynamic is a discipline that describes the behaviour of an electrically conducting fluid in the presence of an electromagnetic field. It is a theory of great interest in a lot of different fields like the study of sunspots, terrestrial magnetism, gas discharges, auroras and interstellar matter.

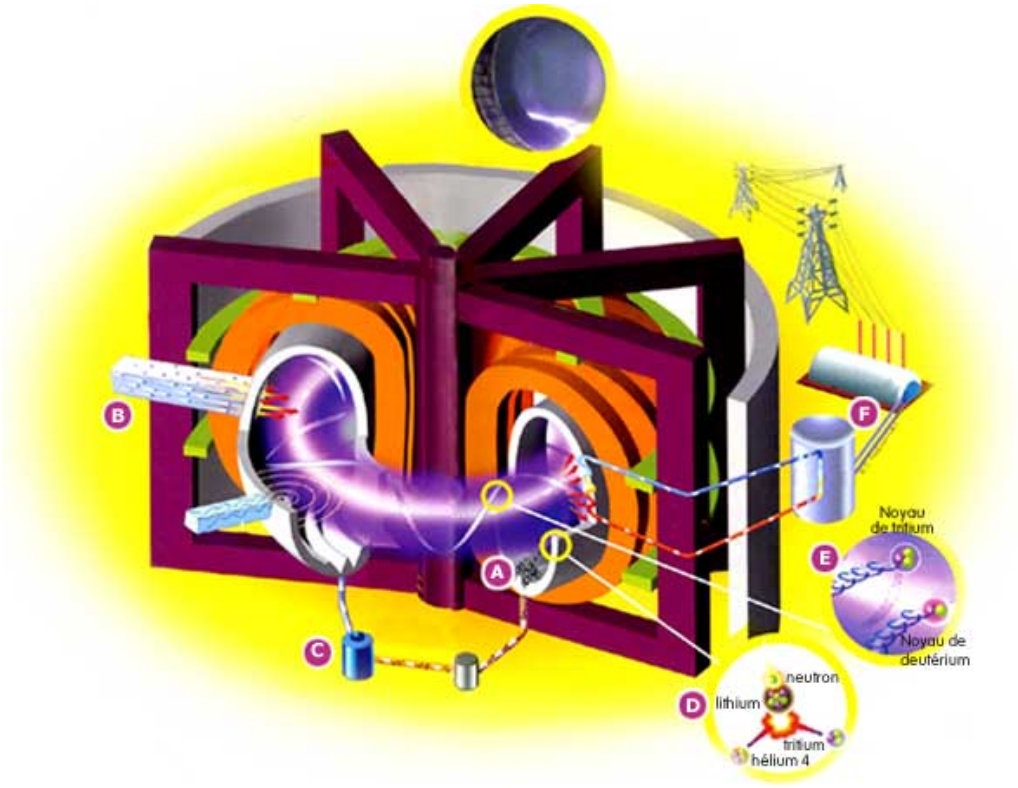

Figure 1: Fusion device (tokamak) with A: the divertor B: the heating system, C: the combustible supply, D: the vessel surrounded by the magnetic coils, E: the lithium blanket, F: the electricity production [36]

In this work, we study three-dimensional MHD equilibria in a way fully compatible with the existence of chaotic magnetic fields. We investigate the existence and stability of good magnetic surfaces with irrational rotational transform[1] that can sustain a pressure jump. Physically, these would form electron transport barriers. The existence of surfaces that satisfy force balance is quite well established [2]. However, the question of the stability to displacements of a 3D interface has not previously been addressed (except for Bernstein *et al* [4] special case of $\beta = \infty$ sharp boundary).

In this paper, we first introduce the theoretical background necessary to understand the problem. Section 2 gives a non-exhaustive overview of the studies done so far on the stability at the interface in a multi-region plasma with a discontinuous pressure profile. We compute the first and second variations of the

[1]the rotational transform is the number of poloidal transits (p) divided by the mean number of toroidal transits (q) of a field line on a toroidal flux surface.

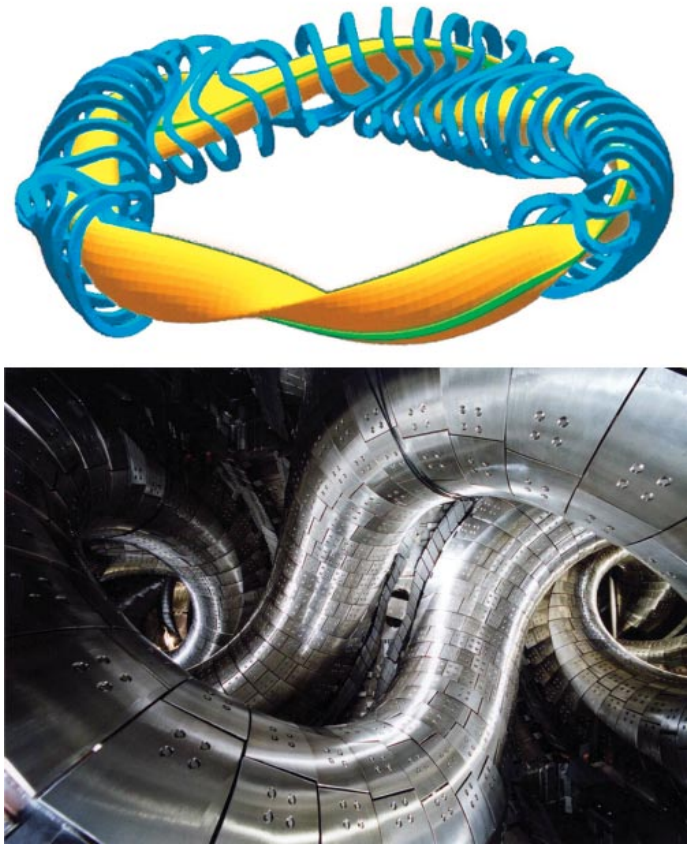

Figure 2: Top : the complex coils of the stellarator W7X. Bottom: a view inside the Japanese Large Helical Device (LHD)[37]

energy while applying a displacement in subsection 2.3 and present in details the stability of pressure jump surface to short-wavelength modes in section 3. We then focus on the stability at zero magnetic shear in sections 4 - 6 and finish by implementing the results on a test case in 7.

2. Theoretical review

2.1. Toroidal plasma equilibrium in 3 dimensions

A good way of modeling toroidal fusion plasma steady state [35] is to consider the three following equations, in SI units:

$$\nabla p = \boldsymbol{J} \times \boldsymbol{B} \tag{1}$$

$$\nabla \times \boldsymbol{B} = \mu_0 \boldsymbol{J} \tag{2}$$

$$\nabla \cdot \boldsymbol{B} = 0 \tag{3}$$

where the first one represents the force balance for the total pressure p, the second is Ampère's law and the third one is the Gauss's law for magnetism. There are 2 main problems that arise in a 3D equilibrium:

- Magnetic islands form on rational flux surface. The field is chaotic around magnetic islands and ergodically fills island separatrix region. Fortunately, not all flux surfaces are destroyed.
- 3-dimensional equilibria have current singularities if $\nabla p \neq 0$

In the present approach, the 3D MHD solvers are built on the premise that the volume is foliated with toroidal magnetic flux surfaces (VMEC [31]), or adapt the magnetic grid to compensate for proximity to low order rational surfaces (PIES [32]). Unfortunately, these solvers cannot rigorously solve ideal MHD and the error usually manifests as a lack of convergence [33]-[34]. Indeed, all experimentally realizable devices encounter symmetry-breaking perturbations and it has been shown [9] that the magnetic field lines are chaotic in a 3-dimensional device such as a tokamak or a stellarator. In this paper we thus try to develop a theory that is structurally stable against these symmetry-breaking perturbations.

2.2. Ideal and relaxed MHD multi-region plasma

Let us first recall here an important result of the Kolmogorov, Arnold and Moser (KAM) theorem [11]. This theorem predicts that, in the case of symmetry-breaking perturbations of the magnetic field, flux surfaces with a sufficiently irrational rotational transform can exist.

Let us focus now on a self-consistent MHD equilibrium. In this case, it is convenient to consider an equilibrium consisting of regions in which the magnetic field is completely chaotic. These regions are separated by perfect flux surfaces, the KAM barriers or interfaces (see figure 3).

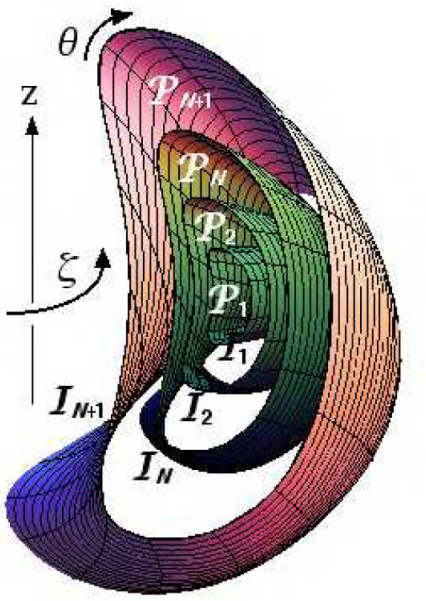

Figure 3: Nested plasma regions, P_i, separated by N toroidal interfaces, I_i, and a fixed wall I_{N+1}, for the case $N = 3$. [8]

As stated before, the flux surfaces form only at irrational rotational transform. We consider a configuration where the pressure gradient ∇p is equal to zero everywhere in the plasma, except for the interfaces with irrational rotational transform where a pressure difference can be supported. This implies that we obtain a step function for the pressure profile [7] where the pressure and rotational transform steps are positioned at flux surface interfaces.

In regions of constant pressure, the magnetic field can be described using the Beltrami equation

$$\mu \boldsymbol{B} = \boldsymbol{\nabla} \times \boldsymbol{B} \tag{4}$$

Which implies that the relation

$$\boldsymbol{J} \times \boldsymbol{B} = 0 \tag{5}$$

is verified if and only if we consider a force free field. If we now apply the divergence operator on both sides of equation 4, we notice that the right-hand side vanishes

$$\boldsymbol{\nabla}\mu \cdot \boldsymbol{B} + \mu \boldsymbol{\nabla} \cdot \boldsymbol{B} = \boldsymbol{\nabla} \cdot \boldsymbol{\nabla} \times \boldsymbol{B} = 0 \tag{6}$$

Using Maxwell's equation

$$\boldsymbol{\nabla} \cdot \boldsymbol{B} = 0 \tag{7}$$

we see that $\boldsymbol{\nabla}\mu = 0$ and thus μ is constant on a field line. The only solution in an ergodic region is thus μ = const everywhere. It can also be a particular solution when $\boldsymbol{B}$ is not ergodic (NB: 3-dimensional effects cause chaotic regions even without turbulence).

In the Multi-region stepped-pressure-profile model, we obtain Beltrami magnetic fields in every region, with different μ_i values in each of them. The Beltrami equation is also used by Taylor [12] arising from his relaxed-MHD variational principle for equilibrium of plasmas that undergo a strongly turbulent phase.

Taylor [12] looked at the relaxation of a plasma that has passed through a phase of strong global overlap of magnetic islands. This overlap of magnetic islands then leads the system to a minimum energy state [17], induced by tearing modes.

Taylor's model was first developed to study strongly turbulent reversed field pinches. But tokamak and stellarator are much more quiescent systems than the reversed field pinches. In these two devices, global island overlap does not occur. The relaxation is thus, at worst, local. When the rotational transform is strongly irrational, island overlap is suppressed and these regions act as robust ideal MHD barriers between the Taylor relaxed states. This leads to the expected equilibria with stepped pressure profile. The pressure jump across the barrier interfaces is counterbalanced by the corresponding magnetic field jumps, which may or may not include jumps in rotational transform.

Taylor's studies show that the main consequence of any small departure from perfect conductivity is that topological properties of the magnetic field are no longer preserved. As a consequence, lines of force may break and coalesce. He showed that during the violent phase of the diffuse pinch, resistivity, microturbulence, inertia or some other departure from perfect conductivity generate a relaxation of the topological constraints. Taylor describes the evolution of a magnetic field in a conducting fluid in a toroidal vessel, in a situation when the resistivity and viscosity are supposed to be small.

The turbulence, allied with small resistivity, allows the plasma to access to a particular minimum energy state in a time very short compared with the usual resistive diffusion time. This is this process that is called plasma relaxation. The system relaxes to the state of lowest energy compatible with the conservation of the total magnetic helicity. The total toroidal magnetic flux should also be conserved.

The wall that encircles the plasma is considered as a magnetic surface too. This allows us to use the Beltrami equation for the vacuum as well. The relaxation process involves the reconnection of magnetic field lines. This is an interesting example of the self-organization of a plasma. This relaxation process can be observed in many different laboratory systems and even in astrophysical plasma [12].

As we have mentioned before, a small departure from perfect conductivity can

make the lines of force break and coalesce. It means that the integral of the scalar product between the magnetic field and the magnetic vector potential $\int \boldsymbol{A} \cdot \boldsymbol{B}$ is not invariant for each line of force. Note that here we have used the vector potential $\boldsymbol{A}$ defined by

$$\boldsymbol{B} = \boldsymbol{\nabla} \times \boldsymbol{A} \tag{8}$$

where $\boldsymbol{A}$ is assume to be a differentiable and single-valued function of position. Even if $\int \boldsymbol{A} \cdot \boldsymbol{B}$ is not invariant for each line of force, the changes in the field topology are only accompanied by very small changes in the field itself. The integral $\int \boldsymbol{A} \cdot \boldsymbol{B}$ over all the field lines will be almost unchanged as long as departures from perfect conductivity are small and that is why $\int \boldsymbol{A} \cdot \boldsymbol{B}$ can be taken as a good invariant on the total volume, even if it is varying on each flux tube [20].

As the plasma is assumed to have a high conductivity, both the temperature and the density are required to be high [16]. But this assumption is in contradiction with the cooling by the wall, and this effect is worsened by the drainage along the magnetic field lines leading to the wall. Unfortunately, such field lines are always present because the assumption that the wall is a magnetic surface cannot totally be met in real experiments.

Further research on the use of RXMHD (Relaxed Magnetohydrodynamics) to model plasmas with magnetic-field-line chaos were undertaken in the last years. Hole *et al* [7] already considered a periodic cylindrical model in which nested flux surfaces exist everywhere. They show that analytic solutions for the magnetic field can be computed when the pressure is constant. They used a variational treatment to construct equilibrium solutions and confirmed previous results from Kaiser and Uecker [13]: stable plasmas can exist in the case of a single-interface configuration if there is a jump in the rotational transform at the plasma-vacuum interface. This can be shown analytically for large n. Hole *et al* compared the stability of a pressureless plasma with only one interface to a plasma with two interfaces in the limit when the two interfaces became arbitrarily close one to the other. Both plasmas have the same net jump in the rotational transform. Hole *et al* found that the two-interface plasma was unstable even when the single-interface plasma was not. Since the single interface models a physical barrier of finite thickness (modelled by the two ι barriers), this suggests that rotational transform jumps should be avoided.

Another point worth being mentioned is that, in the model, the current density must be infinite at any interface where there is a pressure jump. But this is unphysical in a real plasma. Mills *et al* [6] argued that this paradox is due to the assumption of a relaxed-MHD region between the coalescing interfaces, which allows a tearing instability to occur. The single-interface configuration case can instead be compared to a plasma containing a thin but finite ideal region, with constraints on

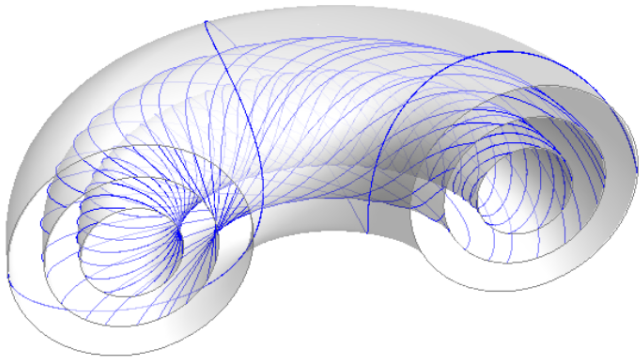

Figure 4: Nested plasma regions, P_i, separated by N toroidal interfaces, I_i, and a fixed wall I_{N+1}, for the case $N = 3$. [39]

the helicity of every field line. Mills *et al* [6] tried to remove the singularity in the current density by considering the pressure and magnetic field to vary continuously between the values on each side of the interface. They showed that if the interface is resolved as an ideal region of non-zero width, the rotational transform profile $\iota(\boldsymbol{r})$ may pass through ideal resonances. The stability analysis must thus consider the structure of the pressure profile in the barrier in the limit that it is spatially resolved.

2.3. RXMHD multi-interfaces plasmas: first and second energy variation

We consider a MHD model of an N-interface plasma as presented on figure 3. Our system comprises N nested plasma regions surrounded by a vacuum region and enclosed by a perfectly conducting wall. We denote P_i the different plasma regions, and V the vacuum region. Each plasma region P_i is encased by the interface I_i. The perfectly conducting wall W surrounds the vacuum region. The interface is a magnetic surface and the magnetic fluxes through any loops in I or W are conserved.

We utilize a variational approach to study the equilibrium and investigate stability. The potential energy (the sum of the thermal and the magnetic energy) of an N-region plasma, where each region is described by either ideal or relaxed MHD, can be written as

$$U_{\text{tot}} = \sum_{i=1}^{N} \left(U_i + \int_{P_i} \frac{\boldsymbol{B}\cdot\boldsymbol{B}}{2\mu_0} d\tau^3 \right) + \int_V \frac{\boldsymbol{B}\cdot\boldsymbol{B}}{2\mu_0} d\tau^3 \tag{9}$$

with

$$U_i = \int_{P_i} \frac{p_i}{\gamma - 1} d\tau^3 \tag{10}$$

In MRXMHD (multi-region relaxed MHD), the interface I_i is assumed to be impermeable to the heat and mass fluxes. All variations are also considered to be slow compared with relaxation timescales. The mass and the entropy are conserved within a plasma region with constant pressure p_i. The potential Energy $U_{\rm tot}$ has to be minimized under two different constraints: the ideal gas law:

$$p_i V_i^{\gamma} = \text{const} \tag{11}$$

and the magnetic helicity constraint:

$$H_{P_i} = \frac{1}{2\mu_0} \int_{P_i} \boldsymbol{A} \cdot \boldsymbol{B} d\tau^3 = \text{const} \tag{12}$$

The mass-entropy [1] (ideal gas) conservation constraint can be expressed in the following way [13]

$$M_i = \int_{P_i} d^3\tau p_i^{1/\gamma} \text{const} \tag{13}$$

This identity is obtained from the relation for an isentropic gas

$$S = \frac{p_i}{\rho^{\gamma}} = \text{const} \tag{14}$$

where ρ denotes the mass density.

Let us now consider the 2 following conditions that hold at a fluid interface.

$$\boldsymbol{n} \times [\![\boldsymbol{E}]\!] = \boldsymbol{n} \cdot \boldsymbol{v} [\![\boldsymbol{B}]\!] \tag{15}$$

$$\boldsymbol{n} \cdot [\![\boldsymbol{B}]\!] = 0 \tag{16}$$

where $\boldsymbol{E}$ is the electric field, $\boldsymbol{B}$ the magnetic field, $\boldsymbol{v}$ the fluid velocity, $\boldsymbol{n}$ the outward pointing unit normal vector and where $[\![X]\!] := X\Big|_{P_{i+1}} - X\Big|_{P_i}$ denotes the jump of a quantity X across I_i. We use the two equations 15-16 and introduce the vector potential $\boldsymbol{A}$

$$\boldsymbol{E} = \frac{\partial \boldsymbol{A}}{\partial t} \tag{17}$$

$$\boldsymbol{B} = \boldsymbol{\nabla} \times \boldsymbol{A} \tag{18}$$

We then introduce the perturbing magnetic field $\boldsymbol{b}$

$$\boldsymbol{b} = \boldsymbol{\nabla} \times (\boldsymbol{\xi} \times \boldsymbol{B}) \tag{19}$$

in P, which can be represented by

$$\boldsymbol{b} = \boldsymbol{\nabla} \times \boldsymbol{a} \tag{20}$$

in V, where $\boldsymbol{a}$ is the perturbed vector potential. Comparing 19 and 20, we notice that we can make the gauge choice

$$\boldsymbol{a} = \boldsymbol{\xi} \times \boldsymbol{B} \tag{21}$$

This choice, called the "Newcomb gauge" in Mills *et al* [6], was shown to be appropriate in both ideal and relaxed MHD, the only difference being the continuation through a mode rational surface. Note that in this paper, the equilibrium quantities are written using capital letters while the perturbations are given by lower case letters. The boundary conditions are then given by

$$\boldsymbol{n} \times \boldsymbol{a}_{\pm} + \xi \boldsymbol{B}_{\pm} = 0 \tag{22}$$

In the previous expression, we used the displacement vector $\boldsymbol{\xi}$ which is determined by

$$\boldsymbol{r} = \boldsymbol{r}_0 + \boldsymbol{\xi} \tag{23}$$

where $\boldsymbol{r}$ is the location of the fluid element at time t, $\boldsymbol{r}_0$ the initial location of the fluid element and we define ξ as

$$\xi = \boldsymbol{\xi} \cdot \boldsymbol{n} \tag{24}$$

Let us now cross equation 22 with the normal vector $\boldsymbol{n}$. We obtain

$$\boldsymbol{n} \times (\boldsymbol{n} \times \boldsymbol{a}_{\pm}) + \xi \boldsymbol{n} \times \boldsymbol{B}_{\pm} = 0 \tag{25}$$

which gives the relation

$$-[\boldsymbol{a}_{\pm} - \boldsymbol{n}(\boldsymbol{n} \cdot \boldsymbol{a}_{\pm})] + \xi \boldsymbol{n} \times \boldsymbol{B}_{\pm} = 0 \tag{26}$$

and thus

$$-\boldsymbol{a}_{\pm \mathrm{tgt}} = \xi \boldsymbol{n} \times \boldsymbol{B}_{\pm} \tag{27}$$

We then follow Spies *et al* [16] and introduce the functional

$$W = \sum_{i=1}^{N} M_{P_i} + M_V - \frac{1}{2} \sum_{i=1}^{N} \mu_i H_{P_i} \tag{28}$$

where H_{P_i} is the helicity and μ_i are Lagrangian multipliers. The terms M_{P_i} and M_V are given by

$$M_{P_i} = \int_{P_i} d^3\tau \frac{1}{2} |\boldsymbol{\nabla} \times \boldsymbol{A}|^2 \tag{29}$$

$$M_V = \int_{V} d^3\tau \frac{1}{2} |\boldsymbol{\nabla} \times \boldsymbol{A}|^2 \tag{30}$$

The constraint of fixed helicity H_{P_i} is observed by varying W instead of U_{tot}. Note that we only consider the magnetic energy and not the thermal energy for the variational approach. We expand W [5] to second order in perturbations from its equilibrium value:

$$W = W_0 + \delta W + \frac{1}{2} \delta^2 W \tag{31}$$

δW is the first variation, linear in the perturbation, and $\delta^2 W$ the second variation, quadratic in the perturbation. *The system is in equilibrium if* $\delta W = 0$ *for every possible displacement of the plasma. Furthermore, the plasma is stable if the second variation* $\delta^2 W$ *is positive for every displacement.*

Since we are interested in the stability at the interface, we need to compute $\delta^2 W$. We first consider the variation of M_{P_i} and use the property

$$\delta \int_{P_i} d^3\tau X = \int_{P_i} d^3\tau \delta X + \int_{I_i} d^2\sigma (\boldsymbol{n}\cdot\boldsymbol{\xi}) X \tag{32}$$

in equation 29. We thus obtain

$$\begin{aligned}\delta M_{P_i} = & \int_{P_i} d^3\tau \boldsymbol{B}\cdot(\boldsymbol{\nabla}\times\boldsymbol{a}) + \frac{1}{2}\int_{I_i} d^2\sigma(\boldsymbol{n}\cdot\boldsymbol{\xi}) B^2_{P_i} \\ & - \frac{1}{2}\int_{I_{i-1}} d^2\sigma(\boldsymbol{n}\cdot\boldsymbol{\xi}) B^2_{P_{i-1}}\end{aligned} \tag{33}$$

We then make use of the identity [16]

$$\begin{aligned}&\int_{P_i} d^3\tau \boldsymbol{B}\cdot(\boldsymbol{\nabla}\times\boldsymbol{a}) - \boldsymbol{a}\cdot(\boldsymbol{\nabla}\times\boldsymbol{B}) \\ &= \int_{I_i} d^2\sigma \boldsymbol{n}\cdot(\boldsymbol{a}\times\boldsymbol{B}) - \int_{I_{i-1}} d^2\sigma \boldsymbol{n}\cdot(\boldsymbol{a}\times\boldsymbol{B})\end{aligned}$$

and considering the boundary conditions 22, we get

$$\begin{aligned}\delta M_{P_i} = & \int_{P_i} d^3\tau \boldsymbol{a}\cdot(\boldsymbol{\nabla}\times\boldsymbol{B}) - \frac{1}{2}\int_{I_i} d^2\sigma(\boldsymbol{n}\cdot\boldsymbol{\xi}) B^2_{P_i} \\ & + \frac{1}{2}\int_{I_{i-1}} d^2\sigma(\boldsymbol{n}\cdot\boldsymbol{\xi}) B^2_{P_{i-1}}\end{aligned} \tag{34}$$

Similarly, we find, for the vacuum

$$\delta M_V = \int_V d^3\tau \boldsymbol{a}\cdot(\boldsymbol{\nabla}\times\boldsymbol{B}) + \frac{1}{2}\int_{I_N} d^2\sigma(\boldsymbol{n}\cdot\boldsymbol{\xi}) B^2_V \tag{35}$$

The helicity variation is obtained following the same method [16]:

$$\begin{aligned}\delta H_{P_i} = & 2\int_{P_i} d^3\tau \boldsymbol{a}\cdot\boldsymbol{B} + \int_{I_i} d^2\sigma(\boldsymbol{n}\times\boldsymbol{A}_{P_i})\cdot(-\boldsymbol{a}_{P_i} + \boldsymbol{\xi}\times\boldsymbol{B}_{P_i}) \\ & - \int_{I_{i-1}} d^2\sigma(\boldsymbol{n}\times\boldsymbol{A}_{P_{i-1}})\cdot(-\boldsymbol{a}_{P_{i-1}} + \boldsymbol{\xi}\times\boldsymbol{B}_{P_{i-1}})\end{aligned} \tag{36}$$

The second and third term on the right-hand side of the equation vanish because of the boundary condition 22, and we are left with

$$\delta H_{P_i} = 2\int_{P_i} d^3\tau \boldsymbol{a}\cdot\boldsymbol{B} \tag{37}$$

Putting everything together, we get

$$\delta W = \sum_{i=1}^{N} (\delta W_{P_i} + \delta W_{I_i}) + \delta W_V \tag{38}$$

where

$$\delta W_{P_i} = \int_{P_i} d^3\tau \boldsymbol{a} \cdot (\boldsymbol{\nabla} \times \boldsymbol{B} - \mu \boldsymbol{B}) \tag{39}$$

$$\delta W_V = \int_V d^3\tau \boldsymbol{a} \cdot (\boldsymbol{\nabla} \times \boldsymbol{B}) \tag{40}$$

And where, at the interface,

$$\delta W_{I_i} = \int_{I_i} \boldsymbol{d^2\sigma} \cdot [(B^2_{P_{i+1}} - B^2_{P_i})\boldsymbol{\xi}] \tag{41}$$

for $i = 1, 2, ..., N-1$ and

$$\delta W_{I_i} = \int_{I_i} \boldsymbol{d^2\sigma} \cdot [(B^2_{V} - B^2_{P_i})\boldsymbol{\xi}] \tag{42}$$

for i equal to N. Now, if we set the first variation of the energy functional to zero, we obtain the following system of equations [5]

$$\boldsymbol{\nabla} \times \boldsymbol{B} = \mu \boldsymbol{B} \quad \texttt{in } P_i \tag{43}$$

$$P = \text{const} \quad \texttt{in } P_i \tag{44}$$

$$\boldsymbol{\nabla} \times \boldsymbol{B} = 0 \quad \texttt{in } V \tag{45}$$

$$\boldsymbol{\nabla} \cdot \boldsymbol{B} = 0 \quad \texttt{in } V \tag{46}$$

$$\boldsymbol{n} \cdot \boldsymbol{B} = 0 \quad \texttt{on } I_i \tag{47}$$

$$\left[\!\left[P + \frac{B^2}{2} \right]\!\right] = 0 \quad \texttt{on } I_i \tag{48}$$

$$\boldsymbol{n} \cdot \boldsymbol{B} = 0 \quad \texttt{on } W \tag{49}$$

P_{i+1} is replaced by the vacuum for $i = N$. The boundary conditions $\boldsymbol{n} \cdot \boldsymbol{B} = 0$ on I_i and W are due to the flux constraints with respect to shrinkable loops in I_i and W. The toroidal fluxes $\Psi^{(t)}_{P_i}$ and $\Psi^{(t)}_V$ in P_i and V and the poloidal flux $\Psi^{(p)}_V$ are fixed in non-shrinkable loops:

$$\Psi^{(t)}_{P_i} = \text{const} \tag{50}$$

$$\Psi^{(t)}_{V} = \text{const} \tag{51}$$

$$\Psi^{(p)}_{V} = \text{const} \tag{52}$$

The system 43-49 constitutes a free-boundary problem for the determination of the relaxed state B at the interface I_i.

We can now derive the second variation of the energy, in the case where $\delta W = 0$. Again, we use the property 32 to get [16]:

$$\begin{aligned}\delta^2 W_{P_i} = & \int_{P_i} d^3\tau \delta[\boldsymbol{a}\cdot(\boldsymbol{\nabla}\times\boldsymbol{B}-\mu\boldsymbol{B})] \\ & + \int_{I_i} d^2\sigma(\boldsymbol{n}\cdot\boldsymbol{\xi})[\boldsymbol{a}\cdot(\boldsymbol{\nabla}\times\boldsymbol{B}-\mu\boldsymbol{B})] \\ & - \int_{I_{i-1}} d^2\sigma(\boldsymbol{n}\cdot\boldsymbol{\xi})[\boldsymbol{a}\cdot(\boldsymbol{\nabla}\times\boldsymbol{B}-\mu\boldsymbol{B})] \end{aligned} \tag{53}$$

using the equilibrium equation, the second and the third term vanish and we are left with

$$\delta^2 W_{P_i} = \int_{P_i} d^3\tau \boldsymbol{a}\cdot\delta(\boldsymbol{\nabla}\times\boldsymbol{B}-\mu\boldsymbol{B}) \tag{54}$$

Rewriting $\delta\boldsymbol{B}$ as

$$\delta\boldsymbol{B} = \boldsymbol{b} = \boldsymbol{\nabla}\times\boldsymbol{a} \tag{55}$$

We obtain

$$\delta^2 W_{P_i} = \int_{P_i} d^3\tau \boldsymbol{a}\cdot[\boldsymbol{\nabla}\times(\boldsymbol{\nabla}\times\boldsymbol{a})-\mu(\boldsymbol{\nabla}\times\boldsymbol{a})] \tag{56}$$

Note that here we followed Spies *et al* 's [16] derivation where $\delta\mu$ is considered as neglectable. We then use the identity

$$\begin{aligned}&\int_{P_i} d^3\tau \left[\boldsymbol{a}\cdot\boldsymbol{\nabla}\times(\boldsymbol{\nabla}\times\boldsymbol{a})-|\boldsymbol{\nabla}\times\boldsymbol{a}|^2\right] \\ &= \int_{I_i} d^2\sigma(\boldsymbol{a}\times\boldsymbol{n})\cdot\boldsymbol{\nabla}\times\boldsymbol{a} - \int_{I_{i-1}} d^2\sigma(\boldsymbol{a}\times\boldsymbol{n})\cdot\boldsymbol{\nabla}\times\boldsymbol{a}\end{aligned} \tag{57}$$

Employing the boundary condition $\boldsymbol{n}\times\boldsymbol{a}+(\boldsymbol{n}\cdot\boldsymbol{\xi})\boldsymbol{B}=0$ on the right hand side of the previous equation, we get

$$\begin{aligned}&\int_{P_i} d^3\tau \left[\boldsymbol{a}\cdot\boldsymbol{\nabla}\times(\boldsymbol{\nabla}\times\boldsymbol{a})-|\boldsymbol{\nabla}\times\boldsymbol{a}|^2\right] \\ &= \int_{I_i} d^2\sigma(\boldsymbol{n}\cdot\boldsymbol{\xi})\boldsymbol{B}\cdot\boldsymbol{\nabla}\times\boldsymbol{a} - \int_{I_{i-1}} d^2\sigma(\boldsymbol{n}\cdot\boldsymbol{\xi})\boldsymbol{B}\cdot\boldsymbol{\nabla}\times\boldsymbol{a}\end{aligned} \tag{58}$$

Using this in 56 leads to

$$\begin{aligned}\delta^2 W_{P_i} = & \int_{P_i} d^3\tau \left[|\boldsymbol{\nabla}\times\boldsymbol{a}|^2-\mu\boldsymbol{a}\cdot(\boldsymbol{\nabla}\times\boldsymbol{a})\right] \\ & + \int_{I_i} d^2\sigma(\boldsymbol{n}\cdot\boldsymbol{\xi})\boldsymbol{B}\cdot\boldsymbol{\nabla}\times\boldsymbol{a} - \int_{I_{i-1}} d^2\sigma(\boldsymbol{n}\cdot\boldsymbol{\xi})\boldsymbol{B}\cdot\boldsymbol{\nabla}\times\boldsymbol{a}\end{aligned} \tag{59}$$

Using the same method, we get, for the vacuum region:

$$\delta^2 W_V = \int_V d^3\tau|\boldsymbol{\nabla}\times\boldsymbol{a}|^2 - \int_{I_N} d^2\sigma(\boldsymbol{n}\cdot\boldsymbol{\xi})\boldsymbol{B}_V\cdot\boldsymbol{\nabla}\times\boldsymbol{a}_V \tag{60}$$

We then resort to the property

$$\delta \int_S \boldsymbol{d^2\sigma} \cdot \boldsymbol{X} = \int_S \boldsymbol{d^2\sigma} \cdot (\delta \boldsymbol{X} + \boldsymbol{\xi} \boldsymbol{\nabla} \cdot \boldsymbol{X}) \tag{61}$$

And obtain the variation of the surface term:

$$\delta^2 W_{I_i} = \frac{1}{2} \int_{I_i} \boldsymbol{d^2\sigma} \cdot \{\delta[(B^2_{P_{i+1}} - B^2_{P_i})\boldsymbol{\xi}] + \boldsymbol{\xi}(\boldsymbol{\nabla} \cdot [(B^2_{P_{i+1}} - B^2_{P_i})\boldsymbol{\xi}])\} \tag{62}$$

P_{i+1} is replaced by V for $i = N$, here and in the following expression. Using the equilibrium equations, we are left with

$$\delta^2 W_{I_i} = \frac{1}{2} \int_{I_i} d^2\sigma (\boldsymbol{n} \cdot \boldsymbol{\xi})[\delta(B^2_{P_{i+1}} - B^2_{P_i}) + \boldsymbol{\xi} \cdot \boldsymbol{\nabla}(B^2_{P_{i+1}} - B^2_{P_i})] \tag{63}$$

We then use the two following properties:

$$\boldsymbol{\xi} \cdot \boldsymbol{\nabla}(B^2_{P_{i+1}} - B^2_{P_i}) = 2(\boldsymbol{n} \cdot \boldsymbol{\xi}) B \, [\![\boldsymbol{n} \cdot \boldsymbol{\nabla} B]\!] \tag{64}$$

and

$$\delta(B^2_{P_{i+1}} - B^2_{P_i}) = 2 \, [\![\boldsymbol{B} \cdot (\boldsymbol{\nabla} \times \boldsymbol{a})]\!] \tag{65}$$

We replace them into 63 to obtain

$$\delta^2 W_{I_i} = \int_{I_i} d^2\sigma (\boldsymbol{n} \cdot \boldsymbol{\xi}) \, [\![\boldsymbol{B} \cdot \boldsymbol{\nabla} \times \boldsymbol{a}]\!] + (\boldsymbol{n} \cdot \boldsymbol{\xi}) \, [\![B \boldsymbol{n} \cdot \boldsymbol{\nabla} B]\!] \tag{66}$$

The first term cancell out with the second and third terms of expressions 59 and 60. Thus, the second variation of the energy is finally given by [5]

$$\delta^2 W = \sum_{i=1}^{N} \delta^2 W_{P_i} + \delta^2 W_{I_i} + \delta^2 W_V \tag{67}$$

with

$$\delta^2 W_{P_i} = \int_{P_i} d^3\tau [|\boldsymbol{\nabla} \times \boldsymbol{a}|^2 - \mu_i \boldsymbol{a^*} \cdot (\boldsymbol{\nabla} \times \boldsymbol{a})] \tag{68}$$

$$\delta^2 W_{I_i} = \int_{I_i} d^3\sigma |\boldsymbol{n} \cdot \boldsymbol{\xi}|^2 \, [\![B \boldsymbol{n} \cdot \boldsymbol{\nabla} B]\!] \tag{69}$$

$$\delta^2 W_V = \int_V d^3\tau |\boldsymbol{\nabla} \times \boldsymbol{a}|^2 \tag{70}$$

where * means the complex conjugation. We are allowed to introduce complex test functions because the functional 67 remains real. Spies [5] states a necessary and sufficient condition for stability ($\delta^2 W > 0$ for all perturbations) as no eigenvalue α of the problem:

$$\boldsymbol{\nabla} \times (\boldsymbol{\nabla} \times \boldsymbol{a}) = \alpha (\boldsymbol{\nabla} \times \boldsymbol{a}) \qquad \texttt{in } P_i \tag{71}$$

$$\boldsymbol{\nabla} \times (\boldsymbol{\nabla} \times \boldsymbol{a}) = 0 \qquad \texttt{in } V \tag{72}$$

$$\boldsymbol{n} \times \boldsymbol{a} = 0 \qquad \texttt{on } W \tag{73}$$

$$\mu \, [\![\boldsymbol{B} \cdot \boldsymbol{\nabla} \times \boldsymbol{a}]\!] + \alpha \, [\![B \boldsymbol{n} \cdot \boldsymbol{\nabla} B]\!] \quad \texttt{on } I_i \tag{74}$$

$$\boldsymbol{n} \times \boldsymbol{a}_{P,V} + \xi \boldsymbol{B}_{P,V} = 0 \qquad \texttt{on } I_N \tag{75}$$

is between zero and μ.

We then follow Kaiser and Uecker [13] and minimize $\delta^2 W$ with respect to $\boldsymbol{a}$. The displacement $\boldsymbol{\xi}$ is kept on the interface and the tangential component of $\boldsymbol{a}$ is fixed thanks to 75. The Euler-Lagrange equations for $\boldsymbol{a}$ are then

$$\boldsymbol{\nabla} \times (\boldsymbol{\nabla} \times \boldsymbol{a}) = \mu(\boldsymbol{\nabla} \times \boldsymbol{a}) \quad \texttt{in } P_i \tag{76}$$

$$\boldsymbol{\nabla} \times (\boldsymbol{\nabla} \times \boldsymbol{a}) = 0 \quad \texttt{in } V \tag{77}$$

$$\boldsymbol{n} \times \boldsymbol{a} = 0 \quad \texttt{on } W \tag{78}$$

Now let us come back to equation 68 and try to write it as a surface integral. We first use the condition

$$\boldsymbol{\nabla} \times (\boldsymbol{\nabla} \times \boldsymbol{a}) = \mu(\boldsymbol{\nabla} \times \boldsymbol{a}) \tag{79}$$

to get

$$\delta^2 W_{P_i} = \int_{P_i} d^3\tau(|\boldsymbol{\nabla} \times \boldsymbol{a}|^2 - \boldsymbol{a^*} \cdot \boldsymbol{\nabla} \times (\boldsymbol{\nabla} \times \boldsymbol{a})) \tag{80}$$

Then we resort to the property ([16] equation 51)

$$\begin{aligned} &\int_{P_i} d^3\tau[\boldsymbol{a}^* \cdot \boldsymbol{\nabla} \times (\boldsymbol{\nabla} \times \boldsymbol{a}) - |\boldsymbol{\nabla} \times \boldsymbol{a}|^2] \\ &= \int_{I_i} d^2\sigma(\boldsymbol{a}^* \times \boldsymbol{n}) \cdot (\boldsymbol{\nabla} \times \boldsymbol{a}) \end{aligned} \tag{81}$$

using the boundary condition

$$\boldsymbol{a} \times \boldsymbol{n} = (\boldsymbol{\xi} \cdot \boldsymbol{n})\boldsymbol{B} \tag{82}$$

we get the following expression

$$\begin{aligned} &\int_{P_i} d^3\tau[\boldsymbol{a}^* \cdot \boldsymbol{\nabla} \times (\boldsymbol{\nabla} \times \boldsymbol{a}) - |\boldsymbol{\nabla} \times \boldsymbol{a}|^2] \\ &= \int_{I_i} d^2\sigma(\boldsymbol{\xi}^* \cdot \boldsymbol{n})\boldsymbol{B} \cdot (\boldsymbol{\nabla} \times \boldsymbol{a}) \end{aligned} \tag{83}$$

we can notice that if we replace 83 in 80 we get

$$\delta^2 W_{P_i} = -\int_{I_i} d^2\sigma(\boldsymbol{\xi}^* \cdot \boldsymbol{n}\boldsymbol{B}) \cdot (\boldsymbol{\nabla} \times \boldsymbol{a}) = -\int_{I_i} d^2\sigma \xi^* \boldsymbol{B} \cdot \boldsymbol{b} \tag{84}$$

Which, using

$$\delta^2 W_{I_i} = \int_{I_i} d^2\sigma \left[\!\!\left[|\boldsymbol{n} \cdot \boldsymbol{\xi}|^2 B(\boldsymbol{n} \cdot \boldsymbol{\nabla})B \right]\!\!\right] \tag{85}$$

Gives the following solution at the interface I_i:

$$\delta^2 W = \int_{I_i} d^2\sigma \left[\!\!\left[\xi^* \boldsymbol{B} \cdot \boldsymbol{b} + |\boldsymbol{n} \cdot \boldsymbol{\xi}|^2 B(\boldsymbol{n} \cdot \boldsymbol{\nabla})B \right]\!\!\right] \tag{86}$$

The perturbing magnetic field $\boldsymbol{b} = \boldsymbol{\nabla} \times \boldsymbol{a}$ is then determined by a system of five equations:

$$\boldsymbol{\nabla} \times \boldsymbol{b} = \mu \boldsymbol{b} \qquad \texttt{in } P_i \tag{87}$$

$$\boldsymbol{\nabla} \times \boldsymbol{b} = 0 \qquad \texttt{in } V \tag{88}$$

$$\boldsymbol{\nabla} \cdot \boldsymbol{b} = 0 \qquad \texttt{everywhere} \tag{89}$$

$$\boldsymbol{n} \cdot \boldsymbol{b} = 0 \qquad \texttt{on } W \tag{90}$$

$$\boldsymbol{n} \cdot \boldsymbol{b}_{\boldsymbol{P},\boldsymbol{V}} = \boldsymbol{B}_{\boldsymbol{P},\boldsymbol{V}} \cdot \boldsymbol{\nabla} \xi + \xi \boldsymbol{n} \cdot \boldsymbol{\nabla} \times (\boldsymbol{n} \times \boldsymbol{B}_{\boldsymbol{P},\boldsymbol{V}}) \quad \texttt{on } I_i \tag{91}$$

and the flux conditions are given by [13]

$$\Psi_{P_i}^{(t)} = \oint_{C_s} \boldsymbol{dl} \cdot (\xi \boldsymbol{n} \times \boldsymbol{B}_{\boldsymbol{P_i}}) \tag{92}$$

$$\Psi_{V}^{(t)} = \oint_{C_s} \boldsymbol{dl} \cdot (\xi \boldsymbol{n} \times \boldsymbol{B}_{\boldsymbol{V}}) \tag{93}$$

$$\Psi_{V}^{(p)} = \oint_{C_l} \boldsymbol{dl} \cdot (\xi \boldsymbol{n} \times \boldsymbol{B}_{\boldsymbol{V}}) \tag{94}$$

where C_s and C_l are loops in I_i. s denotes the short way around the torus, l the long way. These two loops are oriented such that $\boldsymbol{n}$, a vector along C_s and a vector along C_l form a right handed system. Coming back to equation 85 we can affirm that the equilibrium is in a relaxed state if

$$\sum_i \int_{I_i} d^2\sigma \left[\!\left[\xi^* \boldsymbol{B} \cdot \boldsymbol{b} + |\xi|^2 B (\boldsymbol{n} \cdot \boldsymbol{\nabla}) B \right]\!\right] \geq 0 \tag{95}$$

for all normal displacement $\boldsymbol{\xi}$ of the interface and corresponding to a magnetic field $\boldsymbol{b}$ as described in equations 87 to 91.

3. Stability of pressure jump surface to short-wavelength modes

Let us now use the $\delta^2 W$ expression derived previously in 67 and write the Lagrangian of our system, considering only the leading order

$$L = \sum_i \int_{P_i} d^3\tau \frac{1}{2}\rho \left\| \dot{\boldsymbol{\xi}} \right\|^2 - \delta^2 W \tag{96}$$

$$L = \sum_i \int_{P_i} d^3\tau \frac{1}{2}\rho\omega^2 \left\| \boldsymbol{\xi} \right\|^2 - \sum_i \int_{P_i} d^3\tau \left\| \boldsymbol{b} \right\|^2 \tag{97}$$

Let us define the displacement $\boldsymbol{\xi}$ as

$$\boldsymbol{\xi}_\pm = \xi_0 \boldsymbol{f}_\pm(x,y) e^{iS_\pm(x,y,z)/\epsilon + i\omega t} \tag{98}$$

where $\boldsymbol{f}, S_\pm, k_\pm \in \mathbb{C}$,[2] where ϵ is an expansion parameter and where the eikonal function $S_\pm$ is given such that

$$\boldsymbol{k}_\pm = \nabla S_\pm \tag{99}$$

The labels $\pm$ are used to specify which side of the interface is considered. The label $-$ corresponds to the inner side (side closest to the magnetic axis) while the sign $+$ corresponds to the outer side (see figure 5). The quantity $\hat{\boldsymbol{\xi}} = \xi_0 \boldsymbol{f}_\pm(x,y)$ is assumed

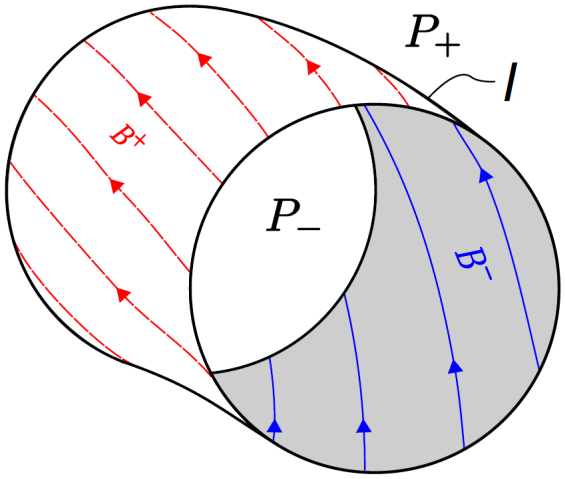

Figure 5: A depiction of a toroidal segment of the surface I [2]

[2] S is complex because we are interested in surface modes - they are oscillatory disturbances of the interface which produce field perturbations that decay exponentially away from the surface.

to vary slowly at the equilibrium length scale. In contrast, the variation of $S_\pm$ is rapid and thus $\|\boldsymbol{k}\|/\epsilon >> 1$, where we define $\|\boldsymbol{k}\|$ the complex norm as

$$\|\boldsymbol{k}\| = \sqrt{\boldsymbol{k}^* \cdot \boldsymbol{k}} \tag{100}$$

The perturbed field potential can be written as[3]

$$\boldsymbol{a}_\pm = \boldsymbol{\xi}_\pm \times \boldsymbol{B}_\pm \tag{101}$$

in "Newcomb gauge" [6]. Furthermore, we have $\boldsymbol{b}_\pm$

$$\boldsymbol{b}_\pm = \boldsymbol{\nabla} \times (\boldsymbol{\xi}_\pm \times \boldsymbol{B}_\pm) \tag{102}$$

Since the variation of $S_\pm$ is rapid, we can write the curl operator using $\boldsymbol{k}$:

$$\boldsymbol{b}_\pm = \frac{i\xi_0 \boldsymbol{k}_\pm}{\epsilon} \times (\boldsymbol{f}_\pm \times \boldsymbol{B}_\pm) e^{iS_\pm/\epsilon} + O(\epsilon^0) \tag{103}$$

And using the property

$$\boldsymbol{a} \times (\boldsymbol{b} \times \boldsymbol{c}) = (\boldsymbol{a} \cdot \boldsymbol{c})\boldsymbol{b} - (\boldsymbol{a} \cdot \boldsymbol{b})\boldsymbol{c} \tag{104}$$

we get

$$\boldsymbol{b}_\pm = \frac{i\xi_0}{\epsilon} (\boldsymbol{k}_\pm \cdot \boldsymbol{B}_\pm \boldsymbol{I} - \boldsymbol{B}_\pm \boldsymbol{k}_\pm) \cdot \boldsymbol{f}_\pm e^{iS_\pm/\epsilon} + O(\epsilon^0) \tag{105}$$

Multiplying by the complex conjugate, we get the norm

$$\begin{aligned} \|\boldsymbol{b}_\pm\|^2 &= \frac{\xi_0^2}{\epsilon^2} [(\boldsymbol{k}_\pm^* \cdot \boldsymbol{B}_\pm)\boldsymbol{f}_\pm^* - (\boldsymbol{k}_\pm^* \cdot \boldsymbol{f}_\pm^*)\boldsymbol{B}_\pm] \\ &\cdot \quad [(\boldsymbol{k}_\pm \cdot \boldsymbol{B}_\pm)\boldsymbol{f}_\pm - (\boldsymbol{k}_\pm \cdot \boldsymbol{f}_\pm)\boldsymbol{B}_\pm] + O(\epsilon) \end{aligned} \tag{106}$$

We then use the Beltrami equation for perturbed magnetic potential

$$\boldsymbol{\nabla} \times (\boldsymbol{\nabla} \times \boldsymbol{a}_\pm) = \mu_\pm \boldsymbol{\nabla} \times \boldsymbol{a}_\pm \tag{107}$$

Again, using the fact that $S_\pm$ is varying fast, we replace the curl operator and obtain

$$\boldsymbol{k}_\pm \times (\boldsymbol{k}_\pm \times \boldsymbol{a}_\pm) = O(\frac{1}{\epsilon}) \tag{108}$$

using 105, we get, to leading order

$$\boldsymbol{k}_\pm \times [(\boldsymbol{k}_\pm \cdot \boldsymbol{B}_\pm)\boldsymbol{I} - \boldsymbol{B}_\pm \boldsymbol{k}_\pm] \cdot \boldsymbol{f}_\pm = 0 \tag{109}$$

where $\boldsymbol{I}$ is the unity matrix. Writing the previous expression more explicitly, we get

$$[(\boldsymbol{k}_\pm \cdot \boldsymbol{B}_\pm)\boldsymbol{k}_\pm \times \boldsymbol{I} - (\boldsymbol{k}_\pm \times \boldsymbol{B}_\pm)\boldsymbol{k}_\pm] \cdot \boldsymbol{f}_\pm = 0 \tag{110}$$

Now let us consider the following expression for $\boldsymbol{k}_\pm$

$$\boldsymbol{k}_\pm = \pm i\delta_\pm \boldsymbol{e}_z + \boldsymbol{k}_{\text{tgt}} \tag{111}$$

[3]Only the normal component $\boldsymbol{\xi} \cdot \boldsymbol{n}$ has a geometrical signifiance - on I, $\boldsymbol{\xi}_+ \cdot \boldsymbol{n} = \boldsymbol{\xi}_- \cdot \boldsymbol{n} = \xi$ determines the displacement of the interface. The tangential components $\boldsymbol{\xi}_{\text{tgt}}^\pm$ are required to give $\boldsymbol{b}$ satisfying the Beltrami equation.

with $\delta_\pm > 0$ and $\boldsymbol{k}_{\text{tgt}} = k^\theta \boldsymbol{e}_\theta + k^\zeta \boldsymbol{e}_\zeta, k^\theta, k^\zeta \in \mathbb{R}$ and $\boldsymbol{e}_z$ a vector perpendicular to the surface. We recall that

$$\boldsymbol{k}_\pm \cdot \boldsymbol{B}_\pm = \boldsymbol{k}_{\text{tgt}} \cdot \boldsymbol{B}_\pm \in \mathbb{R} \tag{112}$$

where we assume that $\boldsymbol{k}_{\text{tgt}}$ and $\boldsymbol{B}_\pm$ are not collinear. Written explicitly, the function $\boldsymbol{f}_\pm$ is given by

$$\boldsymbol{f}_\pm = f_z^\pm \boldsymbol{e}_z + \boldsymbol{f}_{\text{tgt}}^\pm \tag{113}$$

$$\boldsymbol{f}_\pm = f_z^\pm \boldsymbol{e}_z + f_B^\pm \boldsymbol{B}_\pm + f_k^\pm \boldsymbol{k}_{\text{tgt}} \tag{114}$$

Using 110,112 and 114, we get the following expression:

$$[(\boldsymbol{k}_{\text{tgt}} \cdot \boldsymbol{B}_\pm)\boldsymbol{k}_\pm \times \boldsymbol{I} - (\boldsymbol{k}_\pm \times \boldsymbol{B}_\pm)\boldsymbol{k}_\pm] \cdot (f_z^\pm \boldsymbol{e}_z + f_k^\pm \boldsymbol{k}_{\text{tgt}}) = 0 \tag{115}$$

We then multiply 115 by $\boldsymbol{B}_\pm$, and we get

$$(\boldsymbol{k}_{\text{tgt}} \cdot \boldsymbol{B}_\pm)[\boldsymbol{B}_\pm \times (\boldsymbol{k}_{\text{tgt}} \pm i\delta \boldsymbol{e}_z)] \cdot (f_z^\pm \boldsymbol{e}_z + f_k^\pm \boldsymbol{k}_{\text{tgt}}) = 0 \tag{116}$$

Which leads to two different solutions:

$$\boldsymbol{k}_{\text{tgt}} \cdot \boldsymbol{B}_\pm = 0 \tag{117}$$

or

$$(\boldsymbol{e}_z \cdot \boldsymbol{B}_\pm \times \boldsymbol{k}_{\text{tgt}}) \cdot (f_z^\pm + i\delta_\pm f_k^\pm) = 0 \tag{118}$$

using the condition that $\boldsymbol{B}_\pm$ and $\boldsymbol{k}_{\text{tgt}}$ are not collinear, we are left with

$$(f_z^\pm + i\delta_\pm f_k^\pm) = 0 \tag{119}$$

We then start again from 115 but multiply it by $\boldsymbol{e}_z$ this time. We obtain

$$\begin{aligned}&(\boldsymbol{k}_{\text{tgt}} \cdot \boldsymbol{B}_\pm)\boldsymbol{e}_z \cdot \boldsymbol{k}_{\text{tgt}} \times (f_z^\pm \boldsymbol{e}_z + f_k^\pm \boldsymbol{k}_{\text{tgt}}) \\ &-\boldsymbol{e}_z \cdot \boldsymbol{k}_{\text{tgt}} \times \boldsymbol{B}_\pm (\boldsymbol{k}_{\text{tgt}} \pm i\delta_\pm \boldsymbol{e}_z) \cdot (f_z^\pm \boldsymbol{e}_z + f_k^\pm \boldsymbol{k}_{\text{tgt}}) = 0\end{aligned} \tag{120}$$

It appears quite clearly that the first term vanishes. Using the condition that $\boldsymbol{B}_\pm$ and $\boldsymbol{k}_{\text{tgt}}$ are not collinear, we are left with only

$$\pm i\delta_\pm f_z^\pm + f_k^\pm \left\|\boldsymbol{k}_{\text{tgt}}\right\|^2 = 0 \tag{121}$$

We then write 119 and 121 as a matrix

$$\begin{pmatrix} 1 & \mp i\delta_\pm \\ \pm i\delta_\pm & \left\|\boldsymbol{k}_{\text{tgt}}\right\|^2 \end{pmatrix} \begin{pmatrix} f_z^\pm \\ f_k^\pm \end{pmatrix} = \begin{pmatrix} 0 \\ 0 \end{pmatrix} \tag{122}$$

and compute the determinant

$$\det \begin{pmatrix} 1 & \mp i\delta_\pm \\ \pm i\delta_\pm & \left\|\boldsymbol{k}_{\text{tgt}}\right\|^2 \end{pmatrix} = 0 \tag{123}$$

Thus

$$\left\|\boldsymbol{k}_{\text{tgt}}\right\|^2 - \delta_\pm^2 = 0 \tag{124}$$

And finally

$$\delta_{\pm} = \|\boldsymbol{k}_{\mathrm{tgt}}\| \tag{125}$$

This means that the disturbance dies away exponentially (i.e. is evanescent) as we move away from the surface on both sides. Replacing this result into 121, we get

$$f_k^{\pm} = \mp \frac{i f_z^{\pm}}{\|\boldsymbol{k}_{\mathrm{tgt}}\|} \tag{126}$$

We are free to choose $f_B^{\pm} = 0$. Then, using 126, we get

$$\boldsymbol{f}^{\pm} = \left(\boldsymbol{e}_z \mp i \frac{\boldsymbol{k}_{\mathrm{tgt}}}{\|\boldsymbol{k}_{\mathrm{tgt}}\|} \right) f_z^{\pm} = \mp i \frac{\boldsymbol{k}_{\pm}}{\|\boldsymbol{k}_{\mathrm{tgt}}\|} f_z^{\pm} \tag{127}$$

Thus we cannot choose $\boldsymbol{\xi}_+$ and $\boldsymbol{\xi}_-$ to be the same on both sides, only the components in the $\boldsymbol{e}_z$ direction are similar. We can then write

$$\boldsymbol{\xi}_{\pm} = \mp i \frac{\boldsymbol{k}_{\pm}}{\|\boldsymbol{k}_{\mathrm{tgt}}\|} \xi_z \tag{128}$$

where

$$\boldsymbol{k}_{\pm} = \boldsymbol{k}_{\mathrm{tgt}} \pm i \, \|\boldsymbol{k}_{\mathrm{tgt}}\| \, \boldsymbol{e}_z \tag{129}$$

Taking the square of $\boldsymbol{k}_{\pm}$, we get

$$\boldsymbol{k}_{\pm}^2 = 0 \tag{130}$$

Inserting 128 in 102, we obtain

$$\boldsymbol{b}_{\pm} = \pm \frac{\boldsymbol{k}_{\pm} \times (\boldsymbol{k}_{\pm} \times \boldsymbol{B}_{\pm})}{\epsilon \, \|\boldsymbol{k}_{\mathrm{tgt}}\|} \xi_z \tag{131}$$

We then use the property of the double cross product 104 and the fact that $\boldsymbol{k}_{\pm}^2 = 0$ to find

$$\boldsymbol{b}_{\pm} = \mp \boldsymbol{k}_{\pm} \frac{\boldsymbol{k}_{\mathrm{tgt}}}{\epsilon \, \|\boldsymbol{k}_{\mathrm{tgt}}\|} \cdot \boldsymbol{B}_{\pm} \xi_z \tag{132}$$

The norm of $\boldsymbol{b}_{\pm}$ is given by

$$\boldsymbol{b}_{\pm}^* \cdot \boldsymbol{b}_{\pm} = \frac{\boldsymbol{k}_{\pm} \cdot \boldsymbol{k}_{\pm}^*}{\epsilon^2} \left\| \frac{\boldsymbol{k}_{\mathrm{tgt}}}{\|\boldsymbol{k}_{\mathrm{tgt}}\|} \cdot \boldsymbol{B}_{\pm} \right\|^2 \|\xi_z\|^2 \tag{133}$$

But

$$\boldsymbol{k}_{\pm} \cdot \boldsymbol{k}_{\pm}^* = \|\boldsymbol{k}_{\mathrm{tgt}}\|^2 + \|\boldsymbol{k}_{\mathrm{tgt}}\|^2 = 2 \, \|\boldsymbol{k}_{\mathrm{tgt}}\|^2 \tag{134}$$

Thus we obtain

$$\boldsymbol{b}_{\pm}^* \cdot \boldsymbol{b}_{\pm} = 2 \frac{\|\boldsymbol{k}_{\mathrm{tgt}} \cdot \boldsymbol{B}_{\pm}\|^2}{\epsilon^2} \|\xi_z\|^2 \tag{135}$$

We then introduce this result into the L expression (equation 97) and get

$$\rho \omega^2 = 4 \sum_{\pm} \frac{\|\boldsymbol{k}_{\mathrm{tgt}} \cdot \boldsymbol{B}_{\pm}\|^2}{\epsilon^2} \tag{136}$$

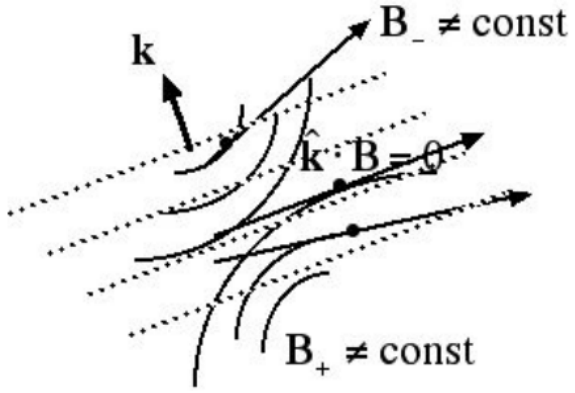

Figure 6: Zero magnetic shear schematic representation

which is strictly positive unless we have

$$\boldsymbol{k}_{\rm tgt} \cdot \boldsymbol{B}_+ = \boldsymbol{k}_{\rm tgt} \cdot \boldsymbol{B}_- = 0 \tag{137}$$

The property 137 is verified only if $\boldsymbol{B}_+$ is parallel or antiparallel to $\boldsymbol{B}_-$ (see figure 6). *It shows that pressure-jump surfaces are stable to short-wavelength modes unless there is at least one point at which the local magnetic shear is zero.* Such points must exist if there is no jump in rotational transform across the surface, i.e. if the global surface magnetic shear is zero at the pressure-jump interface. Previous studies [6] showed that zero rotational transform jump is good for internal stability of a finite-width interface. In the specific case of a cylindrical geometry, if the magnetic shear is zero at one point on the surface, then the local shear is also zero everywhere on the surface. This case is thus very similar to that studied by Bernstein *et al* [4], showing that a cylinder with a decreasing pressure outwards is unstable to high-n flute modes, because the curvature is unfavorable everywhere. If the global magnetic shear at the interface is zero then, in the 2-D, axisymmetric case there will be axisymmetric circles where the local magnetic shear vanishes. In a general 3-D geometry there will also be lines on which the local shear vanishes. In both the 2-D and 3-D cases, it is necessary to extend Bernstein *et al* [4] analysis. That is, we need to expand around the line, or point, of zero shear and construct an envelope function that satisfies the dynamical equations. But before going further, let us consider the $\delta^2 W$ to order ϵ^0 when the local magnetic shear is zero.

4. Stability at zero magnetic shear: theoretical approach

Let us focus our study on a plasma/plasma interface and start with the $\delta^2 W$ equation

$$\delta^2 W = \int_i d^2\sigma \left[\!\left[\xi^* \boldsymbol{B}\cdot\boldsymbol{b} + |\xi|^2 B(\boldsymbol{n}\cdot\boldsymbol{\nabla})B \right]\!\right] \tag{138}$$

where $\boldsymbol{b}_\pm$ is given by

$$\boldsymbol{b}_\pm = \boldsymbol{\nabla}\times(\boldsymbol{f}_\pm\times\boldsymbol{B}_\pm)\xi_0 e^{iS_\pm/\epsilon} \tag{139}$$

$$= \xi_0 e^{iS_\pm/\epsilon}\frac{i\boldsymbol{k}_\pm}{\epsilon}\times(\boldsymbol{f}_\pm\times\boldsymbol{B}_\pm) + \xi_0 e^{iS_\pm/\epsilon}\boldsymbol{\nabla}\times(\boldsymbol{f}_\pm\times\boldsymbol{B}_\pm) \tag{140}$$

We are interested in the cases of zero magnetic shear, where $\boldsymbol{B}\cdot\boldsymbol{b}$ vanishes to highest order, i.e. when

$$\boldsymbol{B}\cdot\boldsymbol{b}_\pm = \xi_0 e^{iS_\pm/\epsilon}\boldsymbol{B}\cdot\boldsymbol{\nabla}\times(\boldsymbol{f}_\pm\times\boldsymbol{B}_\pm) \tag{141}$$

$\delta^2 W$ is then given by

$$\delta^2 W = \int_i d^2\sigma \left[\!\left[\xi_0^2(\boldsymbol{f}^*\cdot\boldsymbol{n})\boldsymbol{B}\cdot\boldsymbol{\nabla}\times(\boldsymbol{f}\times\boldsymbol{B}) + \xi_0^2|\boldsymbol{f}|^2 B(\boldsymbol{n}\cdot\boldsymbol{\nabla})B \right]\!\right] \tag{142}$$

We then follow Bernstein [4] and rewrite the second term of the integral using

$$B_\pm\boldsymbol{n}\cdot\boldsymbol{\nabla}B_\pm = \boldsymbol{n}\cdot\boldsymbol{R}_\pm\frac{\|\boldsymbol{B}_\pm\|^2}{R_\pm^2} \tag{143}$$

with $\boldsymbol{R}_\pm$ the vector from a point on a line of force to the center of curvature field line. Note that, for a point close to zero magnetic shear, $\boldsymbol{R}_+ \approx \boldsymbol{R}_-$. The second variation of the energy is then given by

$$\begin{aligned}\delta^2 W = &\int_i d^2\sigma \left[\!\left[\xi_0^2(\boldsymbol{n}\cdot\boldsymbol{f}^*)\boldsymbol{B}\cdot\boldsymbol{\nabla}\times(\boldsymbol{f}\times\boldsymbol{B}) \right]\!\right] \\ &+ \|\boldsymbol{\xi}_z\|^2\,\boldsymbol{n}\cdot\boldsymbol{R}\frac{\|\boldsymbol{B}_+\|^2 - \|\boldsymbol{B}_-\|^2}{R^2}\end{aligned} \tag{144}$$

If $\boldsymbol{R}$ is directed toward the plasma, the second term of equation 148 has a stabilizing contribution if $\|\boldsymbol{B}_+\|^2 < \|\boldsymbol{B}_-\|^2$ and an unstabilizing contribution if $\|\boldsymbol{B}_+\|^2 > \|\boldsymbol{B}_-\|^2$. On the other hand, if $\boldsymbol{R}$ points away from the plasma, the system is stabilized by the second term if $\|\boldsymbol{B}_+\|^2 > \|\boldsymbol{B}_-\|^2$ and is made more unstable if $\|\boldsymbol{B}_+\|^2 < \|\boldsymbol{B}_-\|^2$

In tokamak or stellarator, the toroidal field is stronger than the poloidal field. The curvature is thus directed approximately towards the Z-axis. The outward normal $\boldsymbol{n}$ is directed away from the magnetic axis. Thus $\boldsymbol{n}\cdot\boldsymbol{R}$ has different signs : on the outboard side farthest from the Z-axis the curvature is unfavorable ($\boldsymbol{n}\cdot\boldsymbol{R} < 0$). By contrast, on the inboard side the curvature is favorable ($\boldsymbol{n}\cdot\boldsymbol{R} > 0$). This is why ballooning modes, i.e. pressure-driven modes which limit the maximum ratio

between the plasma pressure and the magnetic pressure [3], are stronger on the outboard side.

It is common, in plasma physics, to define a field-line curvature vector

$$\boldsymbol{\kappa} = \boldsymbol{e}_{\|} \cdot \boldsymbol{\nabla} \boldsymbol{e}_{\|} \tag{145}$$

where

$$\boldsymbol{e}_{\|} = \frac{\boldsymbol{B}}{\|\boldsymbol{B}\|} \tag{146}$$

It can be proved that $\boldsymbol{\kappa}$ is perpendicular to $\boldsymbol{B}$ or, in other terms, that

$$\boldsymbol{\kappa} \cdot \boldsymbol{B} = 0 \tag{147}$$

This is done in Annexe 10.1. $\delta^2 W$ can be written in terms of $\boldsymbol{\kappa}$

$$\begin{aligned} \delta^2 W = & \int_i d^2\sigma \left[\!\left[\xi_0^2 |\boldsymbol{f}^*| \boldsymbol{B} \cdot \boldsymbol{\nabla} \times (\boldsymbol{f} \times \boldsymbol{B}) \right]\!\right] \\ & + \|\boldsymbol{\xi}_z\|^2 \boldsymbol{n} \cdot \boldsymbol{\kappa} (\|\boldsymbol{B}_+\|^2 - \|\boldsymbol{B}_-\|^2) \end{aligned} \tag{148}$$

Where we identify $\boldsymbol{\kappa}$ as

$$\boldsymbol{\kappa} = \frac{\boldsymbol{R}}{R^2} \tag{149}$$

5. Study of the energy variation using Green's functions

Another approach to the stability problem is to make use of the Green's function method. We give below a short résumé of some interesting ideas and present some new expressions derived. However, deeper investigations and computations still have to be undertaken.

We start by considering the homogeneous Neumann force-free field problem, which is given by

$$\boldsymbol{\nabla} \times \boldsymbol{B} = \mu \boldsymbol{B} \tag{150}$$

in the volume P and by

$$\boldsymbol{n} \cdot \boldsymbol{B} = 0 \tag{151}$$

on the surface ∂P. μ is constant. This problem is equivalent to solving the Dirichlet problem [23] (given here in a cylindrical coordinate system)

$$\frac{\partial}{\partial r}\left(\frac{1}{r}\frac{\partial}{\partial r}(rB_\phi)\right) + \frac{\partial^2 B_\phi}{\partial z} + \mu^2 B_\phi = 0 \tag{152}$$

on the surface S and with the boundary conditions

$$\frac{1}{r}\frac{\partial}{\partial r}(rB_\phi)\boldsymbol{e}_r + \frac{\partial B_\phi}{\partial z}\boldsymbol{e}_z = 0 \tag{153}$$

on the boundary ∂S. The 2 other components of the magnetic field are given by

$$B_r = -\frac{1}{\mu}\frac{\partial B_\phi}{\partial z} \tag{154}$$

and

$$B_z = \frac{1}{\mu r}\frac{\partial}{\partial r}(rB_\phi) \tag{155}$$

The boundary condition 153 is equivalent to

$$rB_\phi = \text{const} \tag{156}$$

on ∂S. Thus, for each μ, there exist axially symmetric solutions to the problem 151-152. We can now derive a boundary integral equation for these axially symmetric solutions. We want this equation to be uniquely solvable for all μ different from a Dirichlet eigenvalue for the problem 152. We thus make use of the following theorem [24]: Let

$$\Phi(\boldsymbol{r}, \boldsymbol{r}') = \frac{1}{4\pi}\frac{e^{i\mu|\boldsymbol{r}-\boldsymbol{r}'|}}{|\boldsymbol{r}-\boldsymbol{r}'|} \tag{157}$$

be the fundamental solution to the Helmoltz equation in 3 dimensions

$$\Delta\Phi = \mu^2\Phi \tag{158}$$

and let our magnetic field $B \in C^1(P) \cap C(\overline{P})$ with $\nabla \cdot B \in C(\overline{P})$. There holds

$$B = -\boldsymbol{\nabla} U + \boldsymbol{\nabla} \times \boldsymbol{A} + \mu \boldsymbol{A} \tag{159}$$

in P where

$$\begin{aligned} U(\boldsymbol{r}) = & \int_P \Phi(\boldsymbol{r}, \boldsymbol{r}') \boldsymbol{\nabla} \cdot \boldsymbol{B}(\boldsymbol{r}') d\boldsymbol{r}' \\ & - \int_S \Phi(\boldsymbol{r}, \boldsymbol{r'}) [\boldsymbol{n}(\boldsymbol{r}') \cdot \boldsymbol{B}(\boldsymbol{r}')] dS(\boldsymbol{r}') \end{aligned} \tag{160}$$

and

$$\begin{aligned} \boldsymbol{A}(\boldsymbol{r}) = & \int_P \Phi(\boldsymbol{r}, \boldsymbol{r}') [\boldsymbol{\nabla} \times \boldsymbol{B}(\boldsymbol{r}') - \mu \boldsymbol{B}] d\boldsymbol{r}' \\ & - \int_S \Phi(\boldsymbol{r}, \boldsymbol{r'}) [\boldsymbol{n}(\boldsymbol{r}') \times \boldsymbol{B}(\boldsymbol{r}')] dS(\boldsymbol{r}') \end{aligned} \tag{161}$$

In our case, $\boldsymbol{\nabla} \cdot \boldsymbol{B} = 0$ in P, $\boldsymbol{n}(\boldsymbol{r}') \cdot \boldsymbol{B}(\boldsymbol{r}') = 0$ on ∂P and $\boldsymbol{\nabla} \times \boldsymbol{B}(\boldsymbol{r}') - \mu \boldsymbol{B} = 0$ and we are only left with

$$\boldsymbol{B}(\boldsymbol{r}) = \boldsymbol{\nabla} \times \boldsymbol{A} + \mu \boldsymbol{A} \tag{162}$$

$$= -(\boldsymbol{\nabla} \times + \mu) \int_S \Phi(\boldsymbol{r}, \boldsymbol{r'}) [\boldsymbol{n}(\boldsymbol{r}') \times \boldsymbol{B}(\boldsymbol{r}')] dS(\boldsymbol{r}') \tag{163}$$

We then use the same approach to find an expression for $\boldsymbol{b}$. We know that $\boldsymbol{\nabla} \cdot \boldsymbol{b} = 0$ in P,
$\boldsymbol{n}(\boldsymbol{r}') \cdot \boldsymbol{b}(\boldsymbol{r}') = \boldsymbol{B} \cdot \boldsymbol{\nabla} \xi + \xi \boldsymbol{n} \cdot \boldsymbol{\nabla} \times (\boldsymbol{n} \times \boldsymbol{B})$ on ∂P and $\boldsymbol{\nabla} \times \boldsymbol{b}(\boldsymbol{r}') - \mu \boldsymbol{b} = 0$. We are thus only left with

$$\begin{aligned} \boldsymbol{b}(\boldsymbol{r}) = & -(\boldsymbol{\nabla} \times + \mu) \int_S \Phi(\boldsymbol{r}, \boldsymbol{r'}) [\boldsymbol{n}(\boldsymbol{r}') \times \boldsymbol{b}(\boldsymbol{r}')] dS(\boldsymbol{r}') \\ & - \boldsymbol{\nabla} \int_S \Phi(\boldsymbol{r}, \boldsymbol{r'}) [\boldsymbol{n}(\boldsymbol{r}') \cdot \boldsymbol{b}(\boldsymbol{r}')] dS(\boldsymbol{r}') \end{aligned} \tag{164}$$

$$\begin{aligned} \boldsymbol{b}(\boldsymbol{r}) = & -(\boldsymbol{\nabla} \times + \mu) \int_S \Phi(\boldsymbol{r}, \boldsymbol{r'}) [\boldsymbol{n}(\boldsymbol{r}') \times \boldsymbol{b}(\boldsymbol{r}')] dS(\boldsymbol{r}') \\ & - \boldsymbol{\nabla} \int_S \Phi(\boldsymbol{r}, \boldsymbol{r'}) \{ \boldsymbol{B}(\boldsymbol{r}') \cdot \boldsymbol{\nabla} \xi(\boldsymbol{r}') \\ & + \xi(\boldsymbol{r'}) \boldsymbol{n}(\boldsymbol{r'}) \cdot \boldsymbol{\nabla} \times [\boldsymbol{n}(\boldsymbol{r}') \times \boldsymbol{B}(\boldsymbol{r'})] \} dS(\boldsymbol{r}') \end{aligned} \tag{165}$$

We want to express $\boldsymbol{b}$ as a function of $\boldsymbol{B}$ and ξ. Let us consider the Fourier transform of $\boldsymbol{b}$

$$\boldsymbol{b}(\boldsymbol{r}) = \int \boldsymbol{b}_k e^{i \boldsymbol{k} \cdot \boldsymbol{r}} dk^3 \tag{166}$$

and of ξ

$$\xi(\boldsymbol{r}) = \int \xi_k e^{i \boldsymbol{k} \cdot \boldsymbol{r}} dk^3 \tag{167}$$

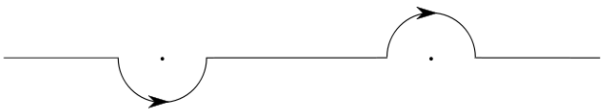

Figure 7: Feynman propagator representation [38]

Furthermore, we notice that the fundamental solution to the Helmoltz equation

$$\Phi(\boldsymbol{r}, \boldsymbol{r}') = \frac{1}{4\pi} \frac{e^{i\mu|\boldsymbol{r}-\boldsymbol{r}'|}}{|\boldsymbol{r}-\boldsymbol{r}'|} \tag{168}$$

satisfies

$$(\boldsymbol{\nabla}^2 + \mu^2)\Phi(\boldsymbol{r}, \boldsymbol{r}') = -\delta(\boldsymbol{r}-\boldsymbol{r}') \tag{169}$$

In particular, the function

$$\Phi_1(\boldsymbol{r}, \boldsymbol{r}') = \frac{-i\mu}{4\pi^2} \int d^3k \frac{e^{i\boldsymbol{k}\cdot(\boldsymbol{r}-\boldsymbol{r}')}}{k^2-\mu^2} \tag{170}$$

is a solution of 169. If we look at the solution of the Helmoltz equation 170, we notice that this solution has two poles at $|\vec{k}| = \pm\mu$. An idea would thus be to use the Feynman propagator, i.e. a contour of integration going under the left pole and over the right pole. For instance, in going from the Fourier-space form of Φ to the real-space form, we can do the k_z integral first. We complete the contour in the lower/upper half plane according as $z - z' > 0$ or $z - z' < 0$. Since we want ϕ to be non-zero for both signs of $z - z'$, there must be a pole in both the upper and lower half k_z plane, as for the Feynman propagator. However, this does not completely resolve the problem, because what we really want to do is to use the surface form of the Green's function solution, in which $\Phi(x - x', y - y', 0)$ needs to be interpreted in a principal part sense, by cutting out a little circle about $x = x', y = y'$ and shrinking it to zero.

Note also that inserting 166, 167 and 170 in our expression for $\boldsymbol{b}$ 165, we get an expression relating $\boldsymbol{b}_k$ to $\boldsymbol{B}$ and ξ_k (see appendix 10.2 for details)

$$\begin{aligned}
&\int \boldsymbol{b}_k e^{i\boldsymbol{k}\cdot\boldsymbol{r}} d\boldsymbol{k} + \frac{1}{4\pi^2}(\boldsymbol{\nabla} \times + \mu) \int d^3k \frac{1}{k^2-\mu^2}(\boldsymbol{n} \times \boldsymbol{b}_k) e^{i\boldsymbol{k}\cdot\boldsymbol{r}} \\
&= \boldsymbol{\nabla} \frac{i\mu}{4\pi^2} \int d^3k \frac{1}{k^2-\mu^2} [i\boldsymbol{B} \cdot \boldsymbol{k}\xi_k \\
&+ \xi_k \boldsymbol{n} \cdot \boldsymbol{\nabla} \times (\boldsymbol{n} \times \boldsymbol{B})] e^{i\boldsymbol{k}\cdot\boldsymbol{r}}
\end{aligned} \tag{171}$$

6. Study of the stability around zero magnetic shear points using a Hamilton-Jacobi theory

As shown previously the plasma at equilibrium is, in general, stable to a deformation. The dominant term of the $\delta^2 W$ equation $\int_{I_i} d^2\sigma \, [\![\xi \boldsymbol{B} \cdot \boldsymbol{b}]\!]$ is always positive, and only goes to zero when $\boldsymbol{B}_+ \| \boldsymbol{B}_-$. We are thus interested in applying deformations at points close to zero magnetic shear, where the curvature term competes with the $\int_{I_i} d^2\sigma \, [\![\xi \boldsymbol{B} \cdot \boldsymbol{b}]\!]$ term. We will thus focus on the study of these special points. To this end, we resort to a code written by M. McGann (paper to be published) which computes the magnetic field on the outer side of an interface, when the field inside the interface and the pressure jump are known. The approach used in the code will be presented in the following sections. But before going further, we need to introduce some theoretical concepts, and, in particular, describe what are the curvilinear coordinates.

6.1. Curvilinear coordinates

To study the equilibrium at the plasma interface, it is useful to resort to curvilinear coordinates. Curvilinear coordinates are a coordinate system for Euclidean space in which the coordinate lines can be curved. Figure 8 shows the difference between curvilinear and Cartesian coordinates in a two dimensional space. In our case, we

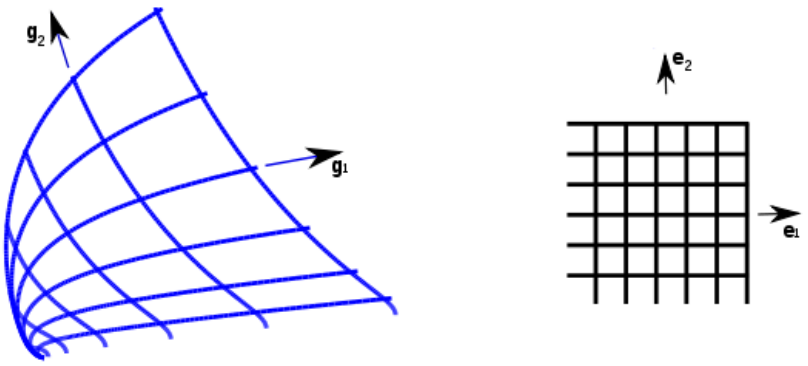

Figure 8: curvilinear and Cartesian coordinates in a two dimensional space [38]

assume a coordinate system θ, ζ, s where the radial coordinate s labels smoothly nested tori, except in the case of the coordinate singularity $s = 0$, which is a topologically circular space curve. The tori $s = \text{const} = s_i$ corresponds to the plasma interface I_i. Thus, $\boldsymbol{e}_s$ is perpendicular to the surface. We then define the 2

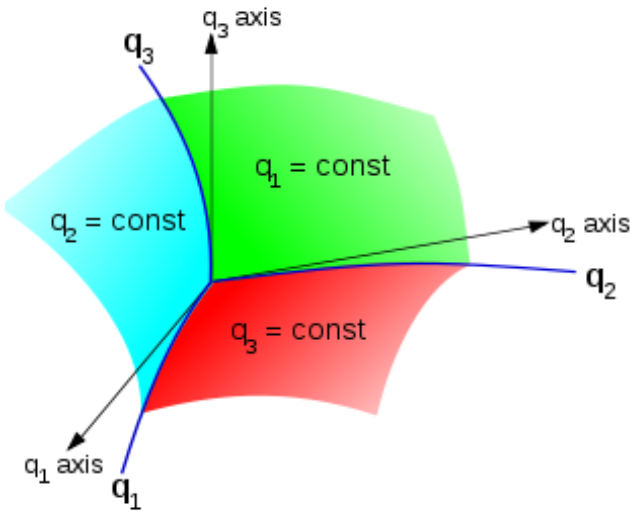

Figure 9: Coordinate surfaces, coordinate lines, and coordinate axes of general curvilinear coordinates [38]

other basis vector $\boldsymbol{e}_\theta$ and $\boldsymbol{e}_\zeta$ where θ and ζ are arbitrary poloidal and toroidal angles, respectively. The directions in which the coordinates θ and ζ increase are chosen such that $(\boldsymbol{e}_\theta, \boldsymbol{e}_\zeta, \boldsymbol{e}_s)$ is a right-handed coordinate system. If $\boldsymbol{r}$ is the position vector of any point in the plasma, we have $\theta = \theta(\boldsymbol{r})$, $\zeta = \zeta(\boldsymbol{r})$ and $s = s(\boldsymbol{r})$. Inverting these relations, we obtain a function $\boldsymbol{R}$

$$\boldsymbol{r} = \boldsymbol{R}(\theta, \zeta, s) \tag{172}$$

The basis vector for the contravariant representation are then given by $(\boldsymbol{e}_\theta, \boldsymbol{e}_\zeta, \boldsymbol{e}_s) = (\partial_\theta \boldsymbol{R}, \partial_\zeta \boldsymbol{R}, \partial_s \boldsymbol{R})$ while the basis vectors for the covariant representation are $(\boldsymbol{e}^\theta, \boldsymbol{e}^\zeta, \boldsymbol{e}^s) = (\boldsymbol{\nabla}\theta, \boldsymbol{\nabla}\zeta, \boldsymbol{\nabla}s)$. The basis vectors can be written more explicitly as follow:

$$\boldsymbol{e}_i = \partial_i \boldsymbol{R} = \frac{\boldsymbol{e}^j \times \boldsymbol{e}^k}{\boldsymbol{e}^\theta \cdot \boldsymbol{e}^\zeta \times \boldsymbol{e}^s} \tag{173}$$

and for the covariant representation:

$$\boldsymbol{e}^i = \boldsymbol{\nabla} u^i = \frac{\boldsymbol{e}_j \times \boldsymbol{e}_k}{\boldsymbol{e}_\theta \cdot \boldsymbol{e}_\zeta \times \boldsymbol{e}_s} \tag{174}$$

Note first that $(\boldsymbol{e}^\theta, \boldsymbol{e}^\zeta, \boldsymbol{e}^s)$ and $(\boldsymbol{e}_\theta, \boldsymbol{e}_\zeta, \boldsymbol{e}_s)$ are mutually reciprocal basis: $\boldsymbol{e}_i \cdot \boldsymbol{e}^j = \delta_i^j$. An arbitrary vector can then either be represented in the covariant representation

$$\boldsymbol{B} = B_i \boldsymbol{e}^i \tag{175}$$

or in the contravariant representation:

$$\boldsymbol{B} = B^i \boldsymbol{e}_i \tag{176}$$

The metric elements are given by

$$\boldsymbol{g}_{ij} = \boldsymbol{e}_i \cdot \boldsymbol{e}_j \tag{177}$$

And

$$\boldsymbol{g}^{ij} = \boldsymbol{e}^i \cdot \boldsymbol{e}^j \tag{178}$$

The metric tensor is used to convert between covariant and contravariant representation by raising or lowering indices:

$$B^i = g^{ij} B_j \tag{179}$$

$$B_i = g_{ij} B^j \tag{180}$$

The Jacobian of the metric tensor takes the form

$$\sqrt{g} = [\det(g_{ij})]^{1/2} = \boldsymbol{e}_\theta \cdot \boldsymbol{e}_\zeta \times \boldsymbol{e}_s = (\boldsymbol{e}^\theta \cdot \boldsymbol{e}^\zeta \times \boldsymbol{e}^s)^{-1} \tag{181}$$

The Jacobian is always positive since we are working with a right-handed set of basis vectors. Now that we have defined the Jacobian, we can give an expression for the volume element appearing in the integration of the energy variation:

$$dV = \sqrt{g} d\theta d\zeta ds \tag{182}$$

The surface area element at the interface I is given by

$$dS = \pm \sqrt{g} \boldsymbol{e}^s(\theta, \zeta, s) d\theta d\zeta \tag{183}$$

The sign depends on whether we are considering an inner or an outer boundary of the region in question. This means that for a region P_i, the sign is negative for I_{i-1} and positive for I_i. In curvilinear coordinate, the gradient is given by

$$\boldsymbol{\nabla} = \boldsymbol{e}^i \partial_i \tag{184}$$

while the divergence takes the form

$$\sqrt{g} \boldsymbol{\nabla} \cdot \boldsymbol{A} = \partial_i (\sqrt{g} A^i) \tag{185}$$

Finally the curl operator is given by

$$\sqrt{g} \boldsymbol{\nabla} \times \boldsymbol{A} = \epsilon_{i,j,k} (\partial_i A_j) \boldsymbol{e}_k \tag{186}$$

where $\epsilon_{i,j,k}$ is the Levi-Civita symbol.

6.2. Hamiltonian development

Let us come back now to the methodology developed by McGann [2] and write the pressure jump equation, at the interface, in terms of the covariant components:

$$2\Delta P = \sum_{i,j\in\{\theta,\zeta\}} g^{ij}[B_i^+ B_j^+ - B_i^- B_j^-] \tag{187}$$

In this geometry, the surface magnetic field is written

$$B^\theta = g^{\theta\theta} B_\theta + g^{\theta\zeta} B_\zeta \tag{188}$$

$$B^\zeta = g^{\theta\zeta} B_\theta + g^{\zeta\zeta} B_\zeta \tag{189}$$

Using that

$$\boldsymbol{B} \cdot \boldsymbol{n} = 0 \tag{190}$$

and

$$(\boldsymbol{\nabla} \times \boldsymbol{B}) \cdot \boldsymbol{n} = 0 \tag{191}$$

we obtain the following result [6]

$$\partial_\theta B_\zeta^\pm - \partial_\zeta B_\theta^\pm = 0 \tag{192}$$

We can thus represent the magnetic field using scalar functions

$$B_\theta^\pm = \partial_\theta f^\pm \tag{193}$$

$$B_\zeta^\pm = \partial_\zeta f^\pm \tag{194}$$

where $f^\pm = \int \boldsymbol{B}^\pm \cdot \boldsymbol{dl}$ are referred to as surface potentials. When known, they fully define the magnetic field on both sides of the interface. We prescribe the field on one side, $\boldsymbol{B}^-$ say, so f^- is treated as known, and f^+ is to be found from the equilibrium condition 187. Using the preceding result, equation 187 can be rewritten as

$$2\Delta P = \sum_{i,j\in\{\theta,\zeta\}} g^{ij}[\partial_\theta f^+ \partial_\zeta f^+ - \partial_\theta f^- \partial_\zeta f^-] \tag{195}$$

which is a partial differential equation for f^+. We want to use an Hamiltonian approach to be able to compute the magnetic field at the outer side of an interface, once we have defined the magnetic field at the inner side. We thus write the pressure jump condition as

$$H(\theta, \zeta, \partial_\theta f^+, \partial_\zeta f^+) = \Delta P \tag{196}$$

where

$$H(\theta, \zeta, p_\theta, p_\zeta) = g^{ij} p_i p_j + V(\theta, \zeta) \tag{197}$$

Here, the potential V is given, in terms of the known potential f^-

$$V(\theta, \zeta) = g^{ij}\partial_i f^- \partial_j f^- \tag{198}$$

and the generalized momenta of the Hamiltonian is

$$p_i = \partial_i f^+ = B_i^+ \tag{199}$$

The partial differential equation 196 can be solved by integrating along its characteristics, which obey Hamilton's equation of motion. Once a solution with the desired irrational number is found, it can be identified with the magnetic field $\boldsymbol{B}^+$

The magnetic field lines can be regarded as trajectories of a $1\frac{1}{2}$ degree of freedom Hamiltonian [2] dynamical system where the toroidal angle ζ is taken to be the analog of time. The half degree of freedom implies that the Hamiltonian depends explicitly on ζ.

The solutions to the Hamiltonian system can be obtained by solving the four characteristic equations [2]

$$\dot{\theta} = \frac{\partial H}{\partial p_\theta} = g^{\theta\theta}p_\theta + g^{\theta\zeta}p_\zeta \tag{200}$$

$$\dot{\zeta} = \frac{\partial H}{\partial p_\zeta} = g^{\theta\zeta}p_\theta + g^{\zeta\zeta}p_\zeta \tag{201}$$

$$\dot{p}_\theta = -\frac{\partial H}{\partial \theta} = \partial_\theta g^{\theta\theta}p_\theta + \partial_\theta g^{\theta\zeta}p_\zeta - \partial_\theta V \tag{202}$$

$$\dot{p}_\zeta = -\frac{\partial H}{\partial \zeta} = \partial_\zeta g^{\theta\zeta}p_\theta + \partial_\zeta g^{\zeta\zeta}p_\zeta - \partial_\zeta V \tag{203}$$

In general, the solution to this Hamiltonian is not unique. To make it unique, we can specify the rotational transform of the field line. The rotational transform, in our case is defined as the limit

$$\iota = \lim_{\Delta\zeta\to\infty} \frac{\Delta\theta}{\Delta\zeta} \tag{204}$$

In action angle coordinate, we can write

$$\iota = \frac{\omega_\Theta}{\omega_z} \tag{205}$$

where

$$\Theta = \omega_\Theta t \tag{206}$$

and

$$Z = \omega_z t \tag{207}$$

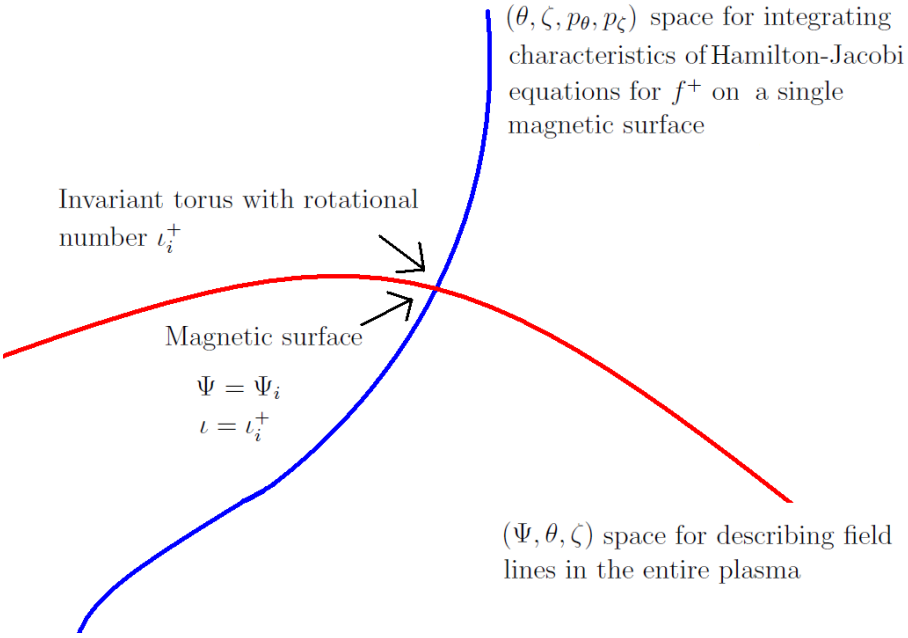

Figure 10: Schematic for the relation of the PJH Hamiltonian and the field line Hamiltonian and their respective phase spaces

These equations are the equations of motion of the system. ω_Θ and ω_z, the poloidal, respectively toroidal angular frequency, are constant. This coordinate system is called straight field line coordinates, because, as its name suggests it, the magnetic field appears as a straight line in this coordinate system. The magnetic potential is then given by

$$f = C_\Theta \Theta + C_z Z + \hat{f}(\theta, \zeta) \tag{208}$$

where C_Θ and C_z are constants and $\hat{f}(\theta, \zeta)$ is a periodic function in θ and ζ:

$$\hat{f} = \sum f_{mn} \sin(m\theta - n\zeta) \tag{209}$$

Let us now come back to the Hamiltonian equations 200 to 203 and rewrite them to simplify the computation of Hamiltonian orbits. We first divide 200 by 201, which imply, as stated before, that we consider the toroidal angle-like coordinate as the "time" variable.

We thus obtain an equation which describes the path of the Hamiltonian trajectory through configuration space

$$\frac{d\theta}{d\zeta} = \frac{g^{\theta\theta} p_\theta + g^{\theta\zeta} p_\zeta}{g^{\theta\zeta} p_\theta + g^{\zeta\zeta} p_\zeta} = \frac{B^{\theta^+}}{B^{\zeta^+}} \tag{210}$$

This is the equation of a magnetic field line on the outer side of the interface[4]. Dividing 202 and 203 by 201, we obtain two equations that relate the canonical momentum with the covariant components of the magnetic field along a Hamiltonian trajectory.

$$\frac{dp_\theta}{d\zeta} = \frac{\partial_\theta g^{\theta\theta} p_\theta + \partial_\theta g^{\theta\zeta} p_\zeta - \partial_\theta V}{g^{\theta\zeta} p_\theta + g^{\zeta\zeta} p_\zeta} \tag{211}$$

$$\frac{dp_\zeta}{d\zeta} = \frac{\partial_\zeta g^{\theta\zeta} p_\theta + \partial_\zeta g^{\zeta\zeta} p_\zeta - \partial_\zeta V}{g^{\theta\zeta} p_\theta + g^{\zeta\zeta} p_\zeta} \tag{212}$$

[4]When an invariant torus in the PJH phase space is found, it can be identified with one side of the interface I, which is a magnetic surface on both sides. Orbits elsewhere in the PJH phase space cannot be identified with physical field lines (see figure 10).

7. Numerical implementation

7.1. PJH code

To solve the Hamiltonian equations, the PJH code resorts to a routine of the NAG library which integrates a system of first-order ordinary differential equations over a specified interval. It uses a fixed order Runge-Kutta method to solve the differential equation problem.

Typical results obtained using McGann's PJH code are presented on figure 11 and 12. Figure 11 shows the variation of the outside field at an interface as we increase the deformation of the interface, in a case when there is no pressure jump. It shows the projection of the field line on the $\zeta = 0$ Poincaré section. The top left picture represents a toroidal perfectly axisymmetric surface. We notice, on this first picture, 2 different kinds of field lines: the ones whose Poincaré section intersection is a continuous line, and the ones that are represented by a discontinuous line on the Poincaré section. The discontinuous lines can be due either to the fact that we need to integrate over a larger number of ζ loops to cover the whole θ range, or simply to the fact that the magnetic field has a rational rotational transform and thus only passes through a specific number of points. We can also identify the points of zero magnetic shear on this figure, where $B_\theta^- = B_\theta^+ = 1$.

When the interface is a deformed torus, the PJH orbits take a less regular shape. If the deformation is big enough, we find orbits for which the intersection with the $\zeta = 0$ Poincaré section gives a closed loop. If we consider bigger deformations, we see that the orbits start having a chaotic behaviour. Note that even if the deformation of the interface is very strong, the intersection of the PJH orbits on the $\zeta = 0$ Poincaré section is still a continuous, or discontinuous line for the points very close to zero magnetic shear. Figure 12 shows the same evolution of the outside magnetic field at an interface as we increase the deformation, but with a pressure jump this time. The pressure at the outer surface is equal to the one at the inner surface diminished by 30%. We see that the trajectories become chaotic much faster than when there is no pressure jump. Furthermore, we notice that even with a very small deformation, we already observe PJH orbits for which the intersection with the $\zeta = 0$ Poincaré section gives a closed loop.

Note that the PJH code written by M. McGann has been benchmarked using the SPEC code from S. Hudson. To make us sure the part we added to this code is physically correct, we did several tests during the programming work that will be detailed below.

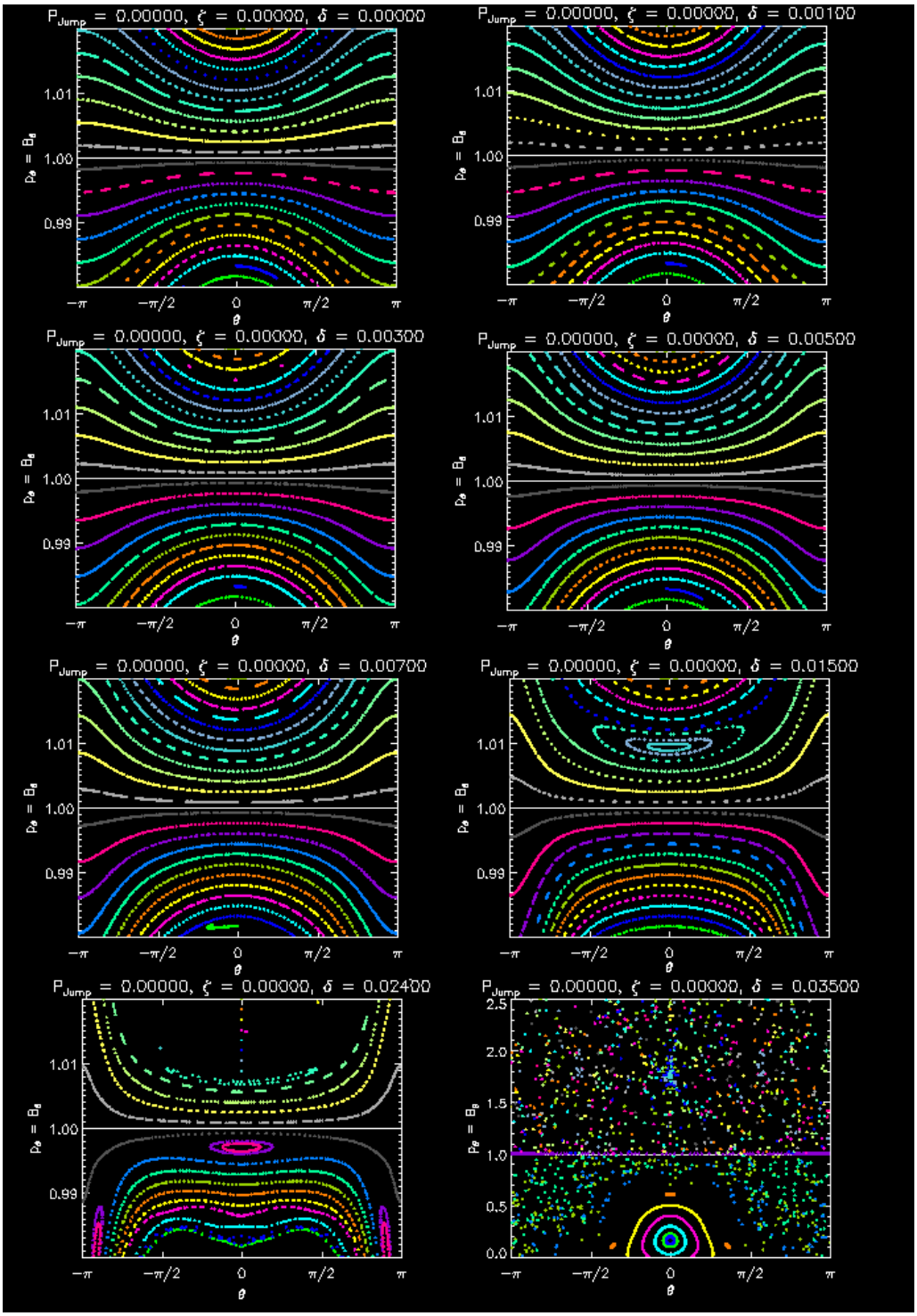

Figure 11: intersection with the $\zeta = 0$ Poincaré section in the case where there is no pressure jump, and for deformations increasing from top left to bottom right

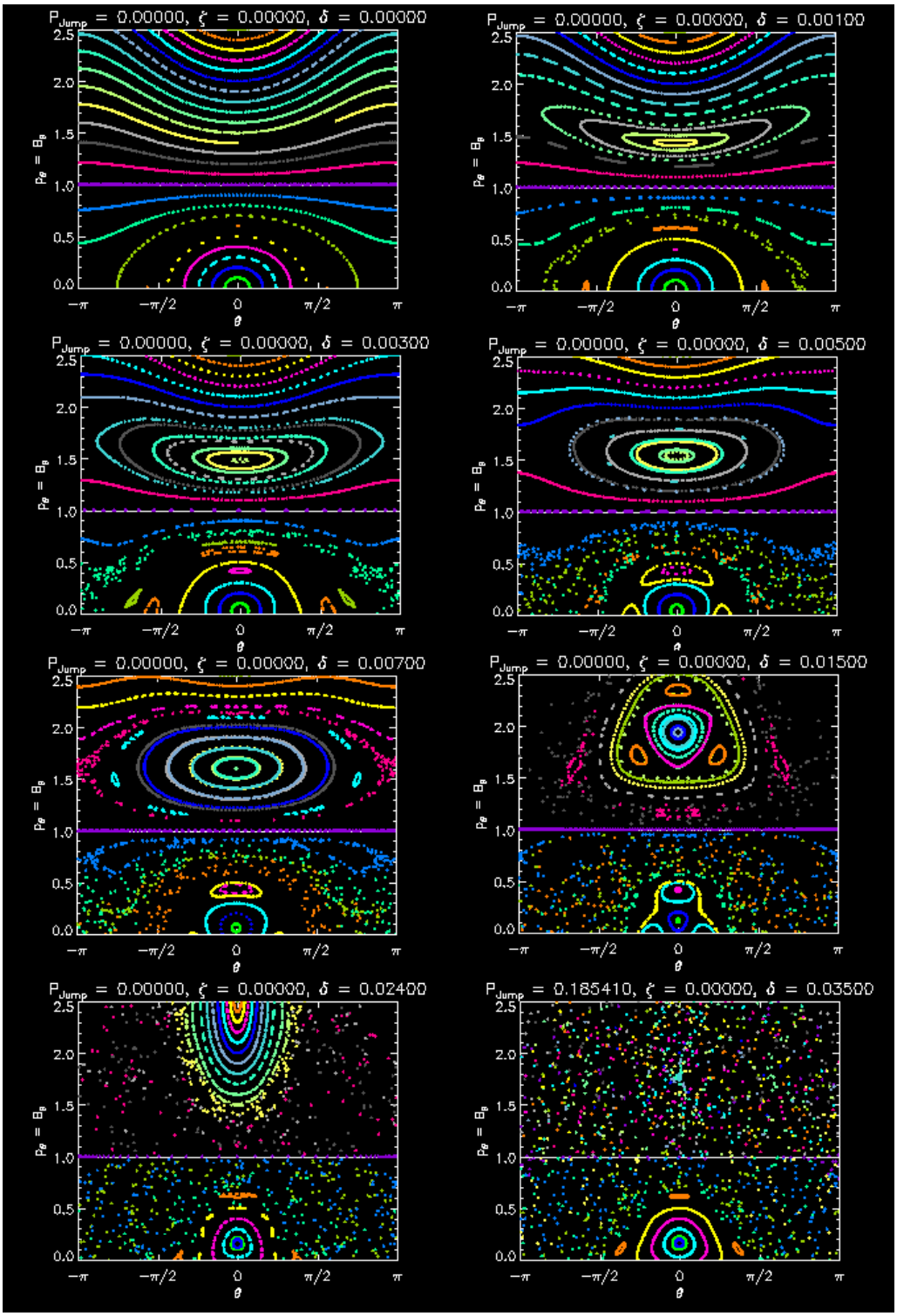

Figure 12: Projection on the $\zeta = 0$ Poincaré section in the case where the pressure at the outer surface is equal to the one at the inner surface diminished by 30%, and for deformations increasing from top left to bottom right

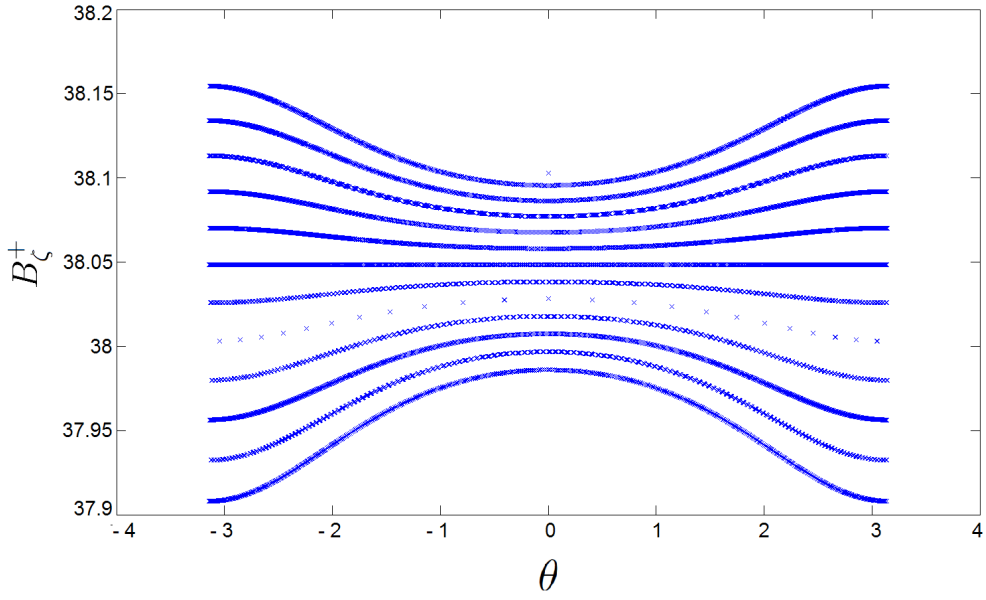

Figure 13: intersection with the $\zeta = 0$ Poincaré section of B_ζ, in the case where the interface is a perfectly axisymmetric torus and when there is no pressure jump.

7.2. ζ component of the magnetic field

We first recall that, in our research, we are especially interested in studying the stability around the points of zero magnetic shear. We thus needed to be able to compute the ratio B_ζ/B_θ at the inner and at the outer interface to find the variation of the rotational transform. That is why we first had to make sure that the ζ component of the magnetic field was reconstructed correctly. Figure 13 shows, as an example, the B_ζ value as a function of θ for $\zeta = 0$ in the case where the interface is a perfectly axisymmetric torus and when there is no pressure jump. We see that B_ζ behaves in an opposite way to B_θ (Figure 11, top left picture), which is logical since the norm of $\boldsymbol{B}$ is conserved when there is no pressure jump.

7.3. Localization of the zero magnetic shear points

Now that we have controlled the accuracy of the ζ component of the magnetic field, we can study the rotational transform variation at the interface. In general, the points of zero magnetic shear will be localized on continuous curves on the surface. This can be seen quite easily from the fact that the points of zero magnetic shear

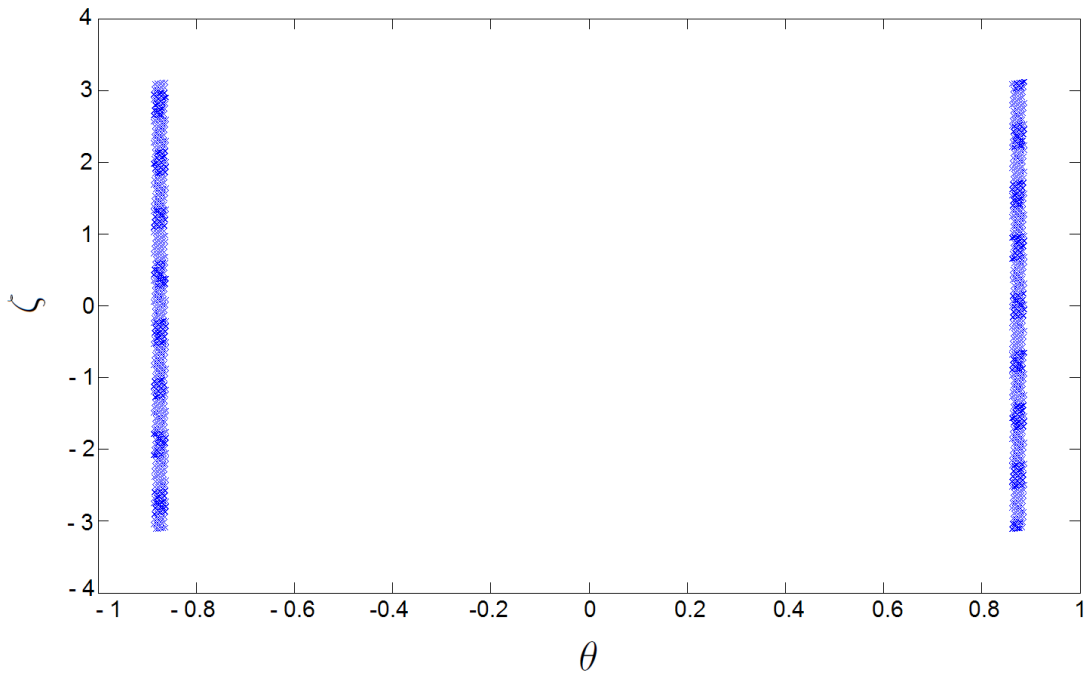

Figure 14: Points close to zero magnetic shear in a toroidal device with no deformation. The points of zero magnetic shear can be found on two circles positioned symmetrically on both side of the horizontal plane

are the $s = 0$ contours of the scalar function:

$$s(\theta, \zeta) \equiv \boldsymbol{n} \cdot \boldsymbol{B}_- \times \boldsymbol{B}_+ \tag{213}$$

In a toroidally symmetric machine like a tokamak these contours will be circles going around the torus the long way. In a poloidally symmetric machine, i.e. a bumpy torus with a large-aspect ratio (ratio of the average major radius to the average minor radius) they would be circles going around the short way. Stellarators for example are normally large aspect ratio devices with the aspect ratio usually being in the range of 7-10 [26]. In a general 3D case, they could also form closed loops not going around the torus either way, but they would almost never degenerate to a single point. Figure 14 shows the points close to zero magnetic shear in a toroidal device. We see clearly that the points of zero magnetic shear can be found on two circles positioned symmetrically on both side of the horizontal plane. Figure 15 shows the points close to zero magnetic shear for a bumpy torus with quite a strong deformation. We see that in this case, the points of zero magnetic shear tend to form a closed loop in the $\zeta = 0$ Poincaré section.

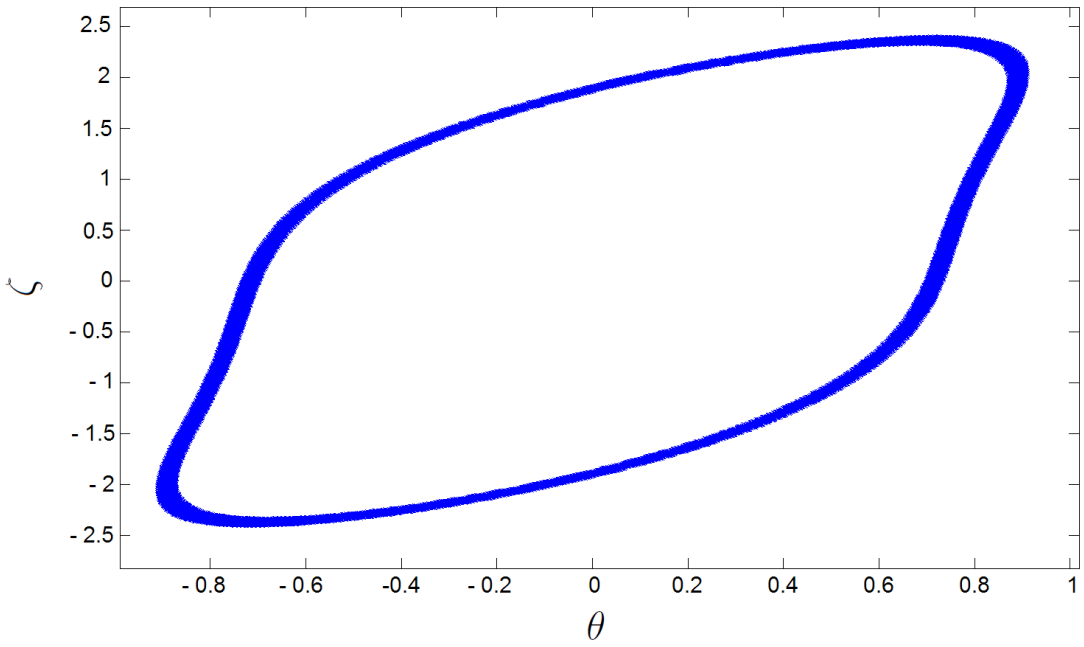

Figure 15: Points close to zero magnetic shear for a bumpy torus with $R_{01} = -Z_{01} = 7 \cdot 10^{-3}$, $R_{21} = Z_{21} = 7 \cdot 10^{-3}$. The points of zero magnetic shear form a close loop in the (θ, ζ) plane.

7.4. 3-dimensional metric

An important element we had to add to McGann's code was to expand the 2-dimensional metric to a 3-dimensional one including a vector normal to the surface. In the code, the general shape of the interface is describe in the following way:

$$x = R_0 \cos(\zeta) + R_1 \cos(\zeta)\cos(\theta) + \sum_{m,n} R_{mn} \cos(m\theta - n\zeta)\cos(\zeta) \quad (214)$$

$$y = R_0 \sin(\zeta) + R_1 \sin(\zeta)\cos(\theta) + \sum_{m,n} R_{mn} \cos(m\theta - n\zeta)\sin(\zeta) \quad (215)$$

$$z = R_1 \sin(\theta) + \sum_{m,n} Z_{mn} \sin(m\theta - n\zeta) \quad (216)$$

with R_0 the toroidal radius of the torus, R_1 the poloidal radius of the torus, and where the deformations of the interface are given by the R_{mn} and Z_{mn} elements. We thus had to specify the R_{mn} and Z_{mn} elements and their derivatives with respect to the normal component. We decided to postulate that the deformation increases linearly as we go away from the center of the plasma region, i.e. we took

$$R_{mn} = C_{mn} s \quad (217)$$

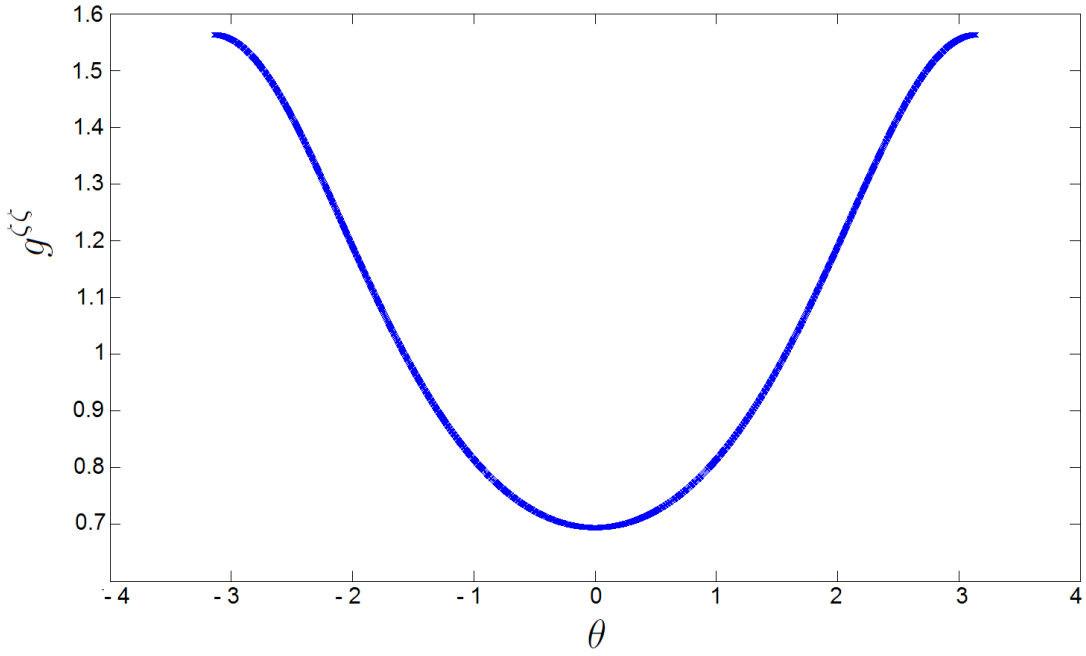

Figure 16: Metric element $g^{\zeta\zeta}$ as a function of θ, in the case where the interface is a perfectly axisymmetric torus without any deformation

$$Z_{mn} = D_{mn} s \tag{218}$$

with C_{mn} and D_{mn} being constants. Thus it follows that

$$\frac{\partial R_{mn}}{\partial s} = C_{mn} \tag{219}$$

$$\frac{\partial Z_{mn}}{\partial s} = D_{mn} \tag{220}$$

And the second derivative is given by

$$\frac{\partial^2 R_{mn}}{\partial s^2} = \frac{\partial^2 Z_{mn}}{\partial s^2} = 0 \tag{221}$$

The g_{ij} metric elements are then obtained after computing the basis vectors $(\boldsymbol{e}_\theta, \boldsymbol{e}_\zeta, \boldsymbol{e}_s)$.

In the case where the interface is a perfectly axisymmetric torus without any deformation, we get $g_{\theta\theta} = \text{const}$, $g^{\theta\theta} = \text{const}$, $g_{ss} = \text{const}$ and $g^{ss} = \text{const}$. The terms $g^{\zeta\zeta}$ and $g_{\zeta\zeta}$ depend on the θ angle, as can be seen on figure 16 and 17. As one would expect, $g_{\zeta\zeta}$ is bigger away from the center of the torus, and smaller close the the center of the torus. $g^{\zeta\zeta}$ has the opposite behaviour. Since our basis vectors are perpendicular to each other, we verify that the other components vanish $g_{\theta\zeta} = g_{\theta s} = g_{\zeta s} = g^{\theta\zeta} = g^{\theta s} = g^{\zeta s} = 0$.

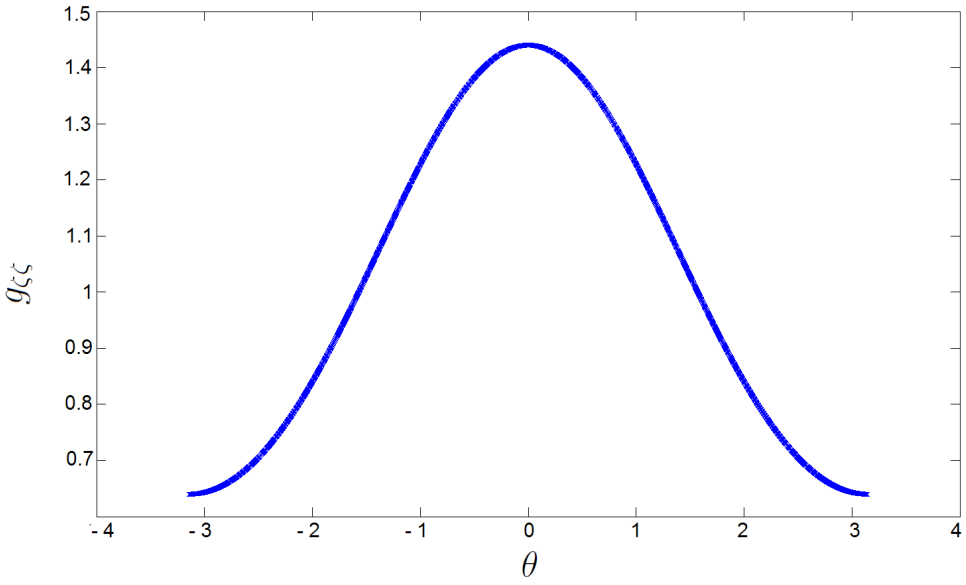

Figure 17: Metric element $g_{\zeta\zeta}$ as a function of θ, in the case where the interface is a perfectly axisymmetric torus without any deformation

Now let us study the case of a surface which is not a perfectly axisymmetric torus. Here we apply the following deformation $R_{01} = -Z_{01} = 5 \cdot 10^{-3}$, $R_{21} = Z_{21} = 5 \cdot 10^{-3}$ to a torus of toroidal radius 1.0 and of poloidal radius 0.2. We verify that $g_{\theta\theta}$, $g^{\theta\theta}$, g_{ss} and g^{ss} are not constant anymore, but vary as a function of θ and ζ. The variation of $g_{\theta\theta}$ is given as an example on figure 18. $g_{\zeta\zeta}$ and $g^{\zeta\zeta}$ also vary as a function of θ and ζ (see figure 19 for $g_{\zeta\zeta}$). The variation is much stronger in the θ than in the ζ direction as the amplitude of the $\boldsymbol{e}_\zeta$ vector mainly depends on the distance to the central axis of the torus. We note further that the terms $g_{\theta s}$ and $g_{\zeta s}$ are not equal to zero anymore, which is due to the way we defined the derivative of R_{mn} and Z_{mn} with respect to s. $g_{\theta\zeta}$ also does not vanish anymore. We can thus conclude by saying the the values obtained for the metric elements are in agreement with our physical intuition.

7.5. Magnetic field derivatives

Now that we have checked the metric used, we can focus on the computation of the magnetic field derivatives. But before going further, let us mention a few important points about the integration method used in the program. To compute the outside magnetic field, we resort to a routine from the NAG library using a Runge-Kutta method to solve the Hamiltonian problem presented in section 6.2. This routine

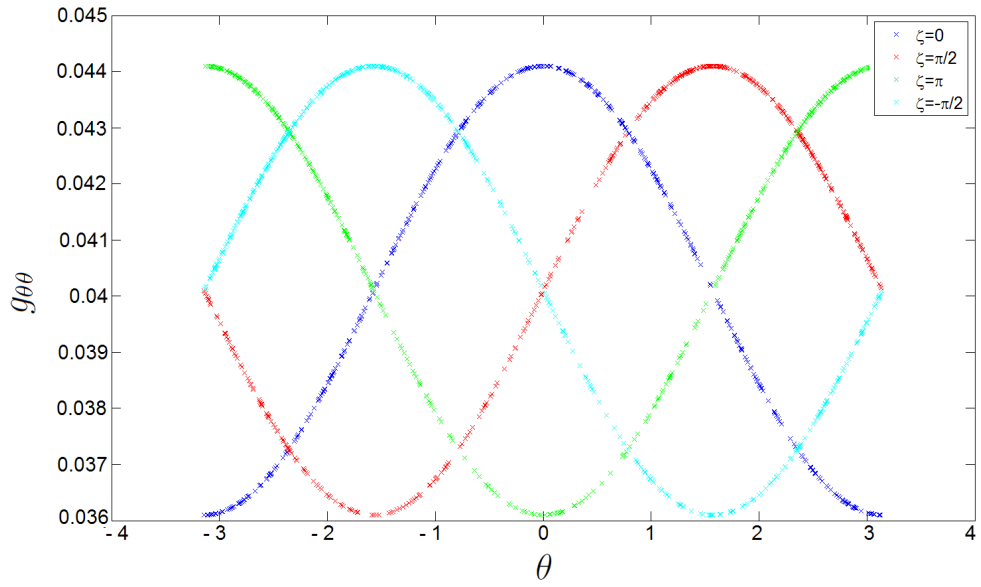

Figure 18: Metric element $g_{\theta\theta}$ as a function of θ and for 4 different ζ, for a deformation $R_{01} = -Z_{01} = 5 \cdot 10^{-3}$, $R_{21} = Z_{21} = 5 \cdot 10^{-3}$ to a torus of toroidal radius 1.0 and of poloidal radius 0.2.

enables us to compute the magnetic field at the outer surface. Note first that if the integration process allows us to specify for which ζ value we want to compute the magnetic field, the θ coordinate is given by the integration along a field line and thus cannot be specified by the user. This implies that the points are not uniformly distributed. Indeed, the number of points close to the vertical axis of the torus tends to be bigger than the number of points on the side of the surface which is the furthest from the central axis. This is an important point that we have to take into account while choosing a method to compute the $\boldsymbol{B}$ derivatives.

The derivatives of $\boldsymbol{B}$ with respect to θ and ζ are indeed important for both the computation of the first and the second term in the $\delta^2 W$ expression 148. We resort to a very simple method to compute the derivatives: for the derivatives relative to θ, we simply look at the 2 closest discrete points having the same ζ value, one being bigger, the other one smaller, and being represented by green squares on figure 23. The θ derivative at the red point on figure 23 is then given by:

$$\frac{d\boldsymbol{B}}{d\theta} = \frac{\boldsymbol{B}_2 - \boldsymbol{B}_1}{\theta_2 - \theta_1} \tag{222}$$

The ζ derivative is obtained from the 4 cyan squares on figure 24. By doing a linear interpolation, we compute the $\boldsymbol{B}$ value at the two virtual points having the same θ

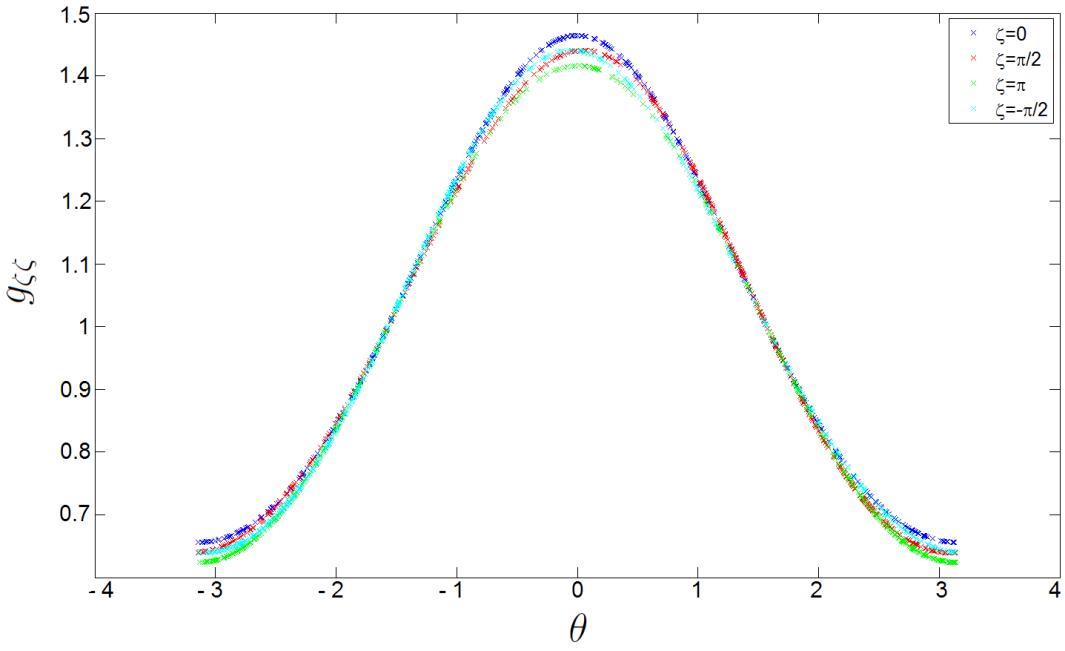

Figure 19: Metric element $g_{\zeta\zeta}$ as a function of θ and for 4 different ζ, for a deformation $R_{01} = -Z_{01} = 5 \cdot 10^{-3}$, $R_{21} = Z_{21} = 5 \cdot 10^{-3}$ to a torus of toroidal radius 1.0 and of poloidal radius 0.2.

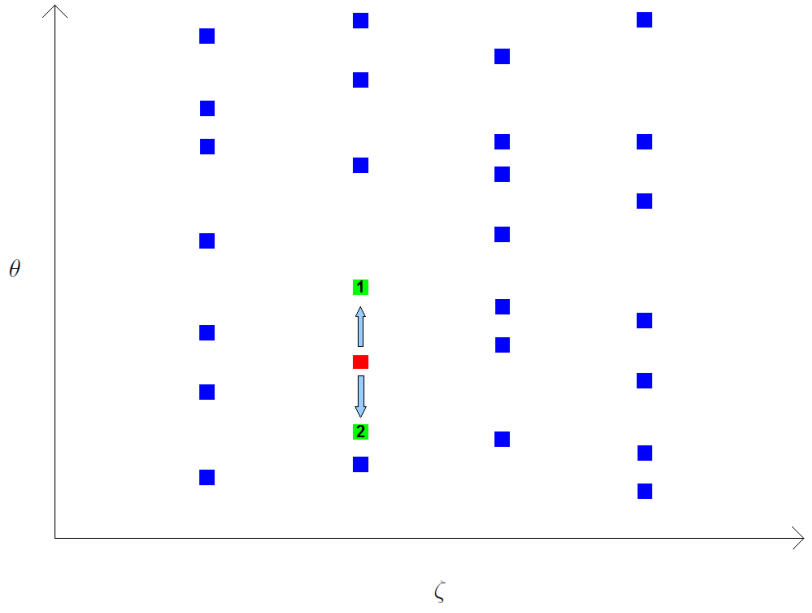

Figure 20: Schematic representation of the way the θ derivatives are computed

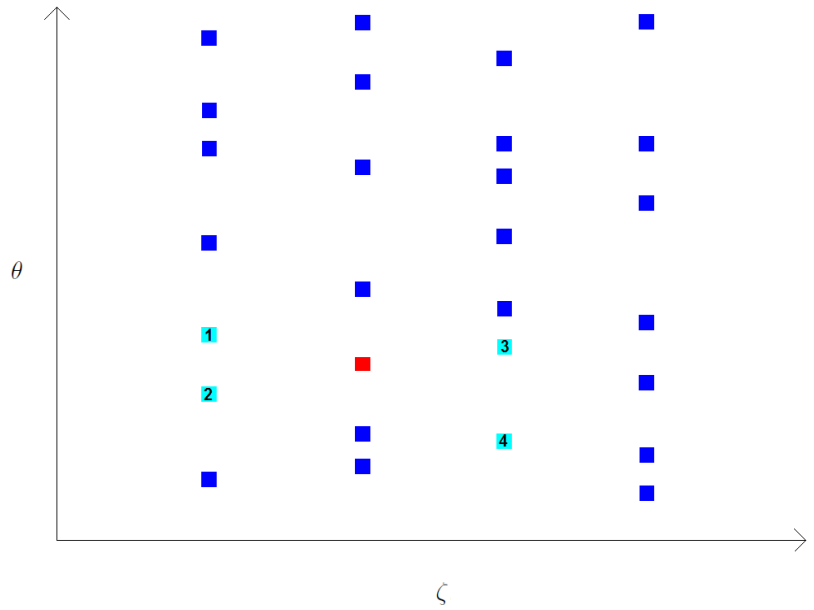

Figure 21: Schematic representation of the way the ζ derivatives are computed

value as the point of interest. These 2 points are modeled by green squares on figure 22. Then from this 2 green points, we get the ζ derivative at the red point by doing

$$\frac{d\boldsymbol{B}}{d\zeta} = \frac{\boldsymbol{B}_6 - \boldsymbol{B}_5}{\zeta_6 - \zeta_5} \tag{223}$$

Figure 23 represents the θ component of the magnetic field as a function of θ, for 3 different ζ. Figure 24 shows the derivatives of B_θ with respect to θ. These 2 figures are obtained for a deformation $R_{01} = -Z_{01} = 3 \cdot 10^{-3}$, $R_{21} = Z_{21} = 5 \cdot 10^{-3}$ to a torus of toroidal radius 1.0 and of poloidal radius 0.2.

As we compare the 2 graphs, we see on the second figure that the derivatives are in good agreement with what is expected when looking at the first figure. Furthermore and as we will show it later in this paper, the small error due to the interpolation process does not influence strongly the final result, especially since, in most of the cases, the term involving the derivative of $\boldsymbol{B}$ with respect to θ and ζ are not dominant ones in the $\delta^2 W$ expression. Similar results are obtained with the ζ derivatives.

There are other methods that could have been used to compute the derivatives. One way is to use an m, n Fourier ansatz for the scalar magnetic potential, and to determine the a_{mn} coefficient to fit the frequency spectrum observed by a point moving on the highest-order periodic orbit. Because the orbit is high-order, it is

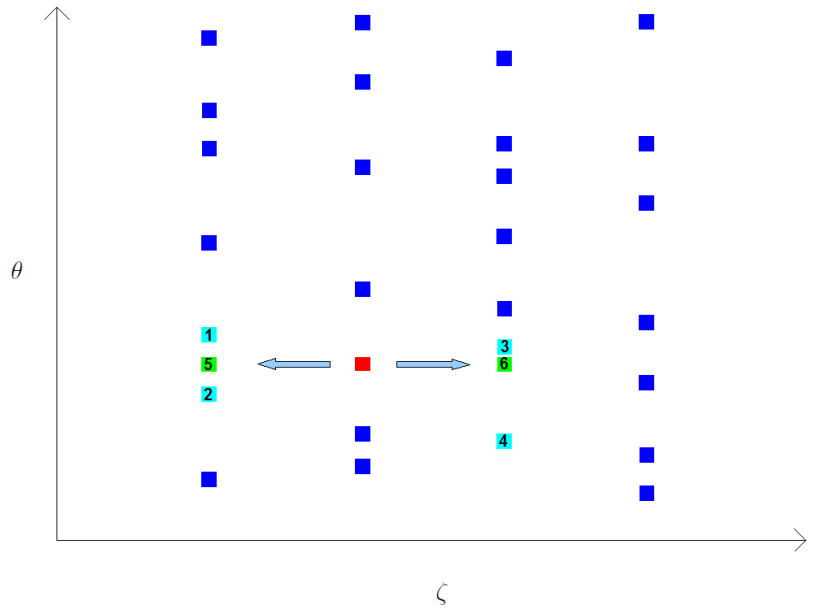

Figure 22: Schematic representation of the way the ζ derivatives are computed

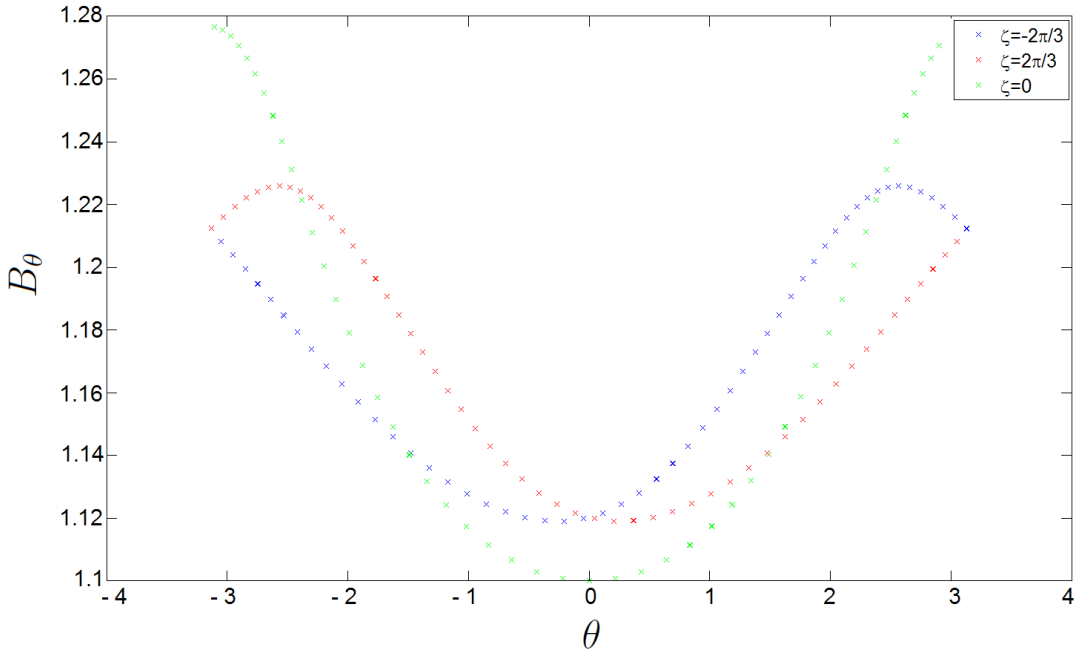

Figure 23: B_θ for a deformation $R_{01} = -Z_{01} = 3 \cdot 10^{-3}$, $R_{21} = Z_{21} = 5 \cdot 10^{-3}$ to a torus of toroidal radius 1.0 and of poloidal radius 0.2

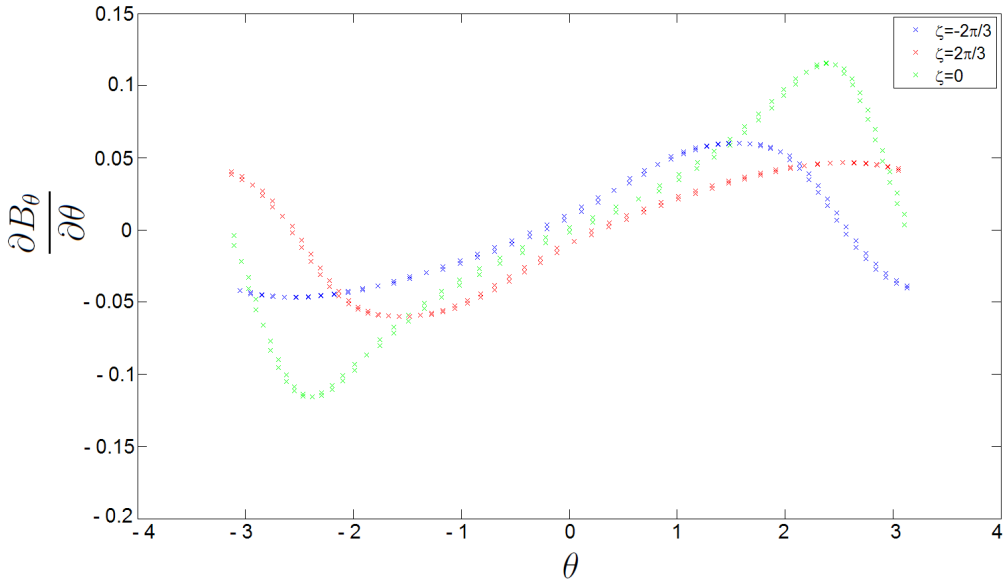

Figure 24: Derivative of B_θ with respect to θ for a deformation $R_{01} = -Z_{01} = 3 \cdot 10^{-3}$, $R_{21} = Z_{21} = 5 \cdot 10^{-3}$ to a torus of toroidal radius 1.0 and of poloidal radius 0.2

effectively irrational and will cover the surface almost ergodically, so there should be enough information to determine all the a_{mn}, provided one truncates at a reasonably low number (this assumes the Fourier spectrum decays rapidly at high m and n, which will break down near criticality). A similar approach is used in [27]. Another approach would be to put the Fourier ansatz into Percival's variational principle [28] and determine the coefficients.

Since the simplest method gave results with good agreement with the expected ones, we just concentrate on this method. We emphasize that the accuracy of the derivatives' computation strongly depends on the number of discrete points covering the surface. The bigger the number of discrete points, the more accurate the integration.

7.6. Study of the curvature term

Let us now study the curvature term. We first verified that the normal vector $\boldsymbol{n}$ was correctly defined. As an example, we show on figure 25 the z component of $\boldsymbol{n}$. Note that all figures presented in this section were obtained for an interface with a deformation $R_{01} = -Z_{01} = 3 \cdot 10^{-3}$, $R_{21} = Z_{21} = 3 \cdot 10^{-3}$ to a torus of toroidal radius 1.0 and of poloidal radius 0.2, and with the outer pressure being equal to the

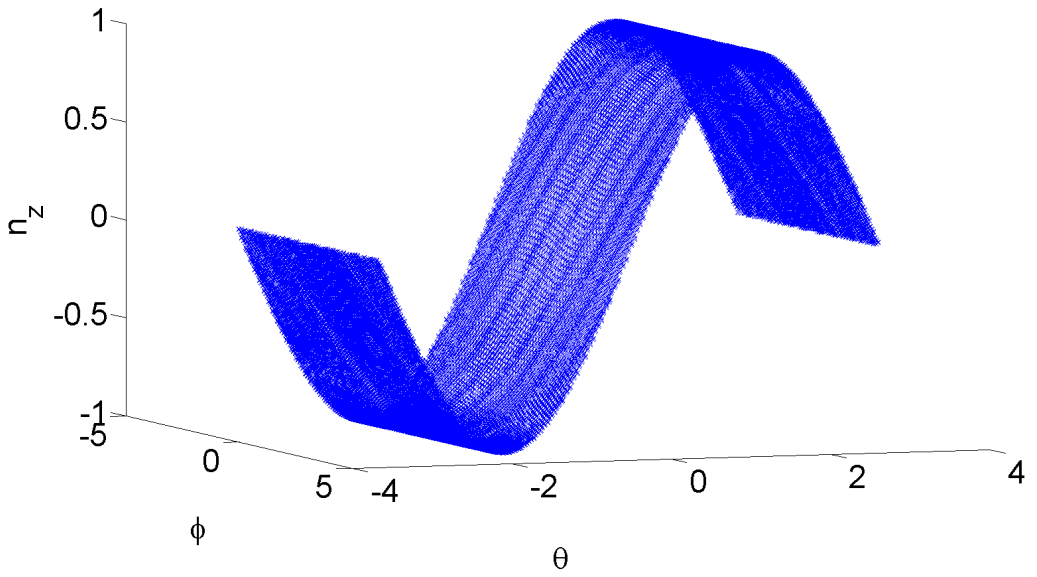

Figure 25: z component of $\boldsymbol{n}$ for a deformation $R_{01} = -Z_{01} = 3 \cdot 10^{-3}$, $R_{21} = Z_{21} = 3 \cdot 10^{-3}$ to a torus of toroidal radius 1.0 and of poloidal radius 0.2

inner pressure -30%. Figure 25 shows that, as expected, the z component of $\boldsymbol{n}$ is mainly dependent on the θ coordinate: positive when θ is positive, negative when θ is negative. The small variations of n_z from a totally sinusoidal behaviour are due to the small deformation of the interface. The accuracy of the x and y component of $\boldsymbol{n}$ were verified in the same way.

We then study the field-line curvature vector $\boldsymbol{\kappa}$, which, in curvilinear coordinates, can be written

$$\begin{aligned}\boldsymbol{\kappa} &= \frac{\boldsymbol{B}}{\|\boldsymbol{B}\|} \cdot \boldsymbol{\nabla} \frac{\boldsymbol{B}}{\|\boldsymbol{B}\|} \\ &= \frac{1}{B^2} \left(g^{\theta\theta} B_\theta \frac{\partial g^{\theta\theta} B_\theta \boldsymbol{e}_\theta}{\partial \theta} + g^{\theta\theta} B_\theta \frac{\partial g^{\zeta\zeta} B_\zeta \boldsymbol{e}_\zeta}{\partial \theta} \right. \\ &\quad \left. g^{\zeta\zeta} B_\zeta \frac{\partial g^{\theta\theta} B_\theta \boldsymbol{e}_\theta}{\partial \zeta} + g^{\zeta\zeta} B_\zeta \frac{\partial g^{\zeta\zeta} B_\zeta \boldsymbol{e}_\zeta}{\partial \zeta} \right)\end{aligned} \tag{224}$$

As we postulated that the toroidal magnetic field component is much stronger than the toroidal field component, we expect the field-line curvature vector to be directed in the direction of the z-axis of the torus. Figure 26 shows the x component of $\boldsymbol{\kappa}$ at the inner surface. We see that the x component of $\boldsymbol{\kappa}$ depends mainly on the ζ angle. κ_x is generally positive when the coordinate x is negative and vice versa (this

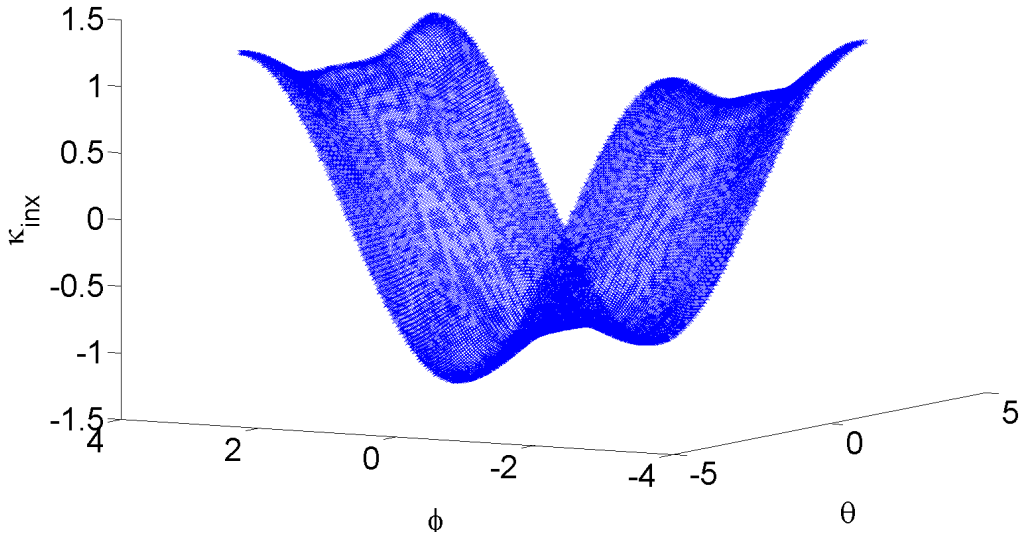

Figure 26: x component of the field-line curvature vector $\boldsymbol{\kappa}$ at the inner interface for a deformation $R_{01} = -Z_{01} = 3 \cdot 10^{-3}$, $R_{21} = Z_{21} = 3 \cdot 10^{-3}$ to a torus of toroidal radius 1.0 and of poloidal radius 0.2

is true as long as the interface has a shape close to axisymmetry, with only little deformations). The y component of $\boldsymbol{\kappa}$ also mainly depends on ζ. In contrast, we verify that the z component of $\boldsymbol{\kappa}$ is mainly dependent on the θ angle, as can be seen on figure 27. κ_z is generally positive when z is negative and vice versa.

If we multiply the normal vector to the interface with the field-line curvature vector, $\boldsymbol{n}\cdot\boldsymbol{k}$, we obtain the results plotted on figures 28, 29 and 30 We first note that the $n_x\kappa_x$ and $n_y\kappa_y$ terms are much bigger then the $n_z\kappa_z$ term. They tend to reach their minimum values when θ is close to zero, and their maximum value when $\theta \approx \pi$. We see that $n_z\kappa_z$ is almost always negative since $\boldsymbol{n}$ points outside the torus while $\boldsymbol{\kappa}$ points in the direction of the vertical axis (z axis). The sum of the 3 components is given on figure 31. This figure proves that the sign of the curvature term depends almost only on θ. $\boldsymbol{\kappa}\cdot\boldsymbol{n}$ is negative away from the z axis (θ close to zero), and positive close to the vertical axis. We obtain the same kind of results while considering $\boldsymbol{\kappa}$ at the outer side of the interface. Note also that $|\boldsymbol{B}_+^2| - |\boldsymbol{B}_-^2| = \Delta P$, thus the sign of the curvature term depends on the form of the pressure profile.

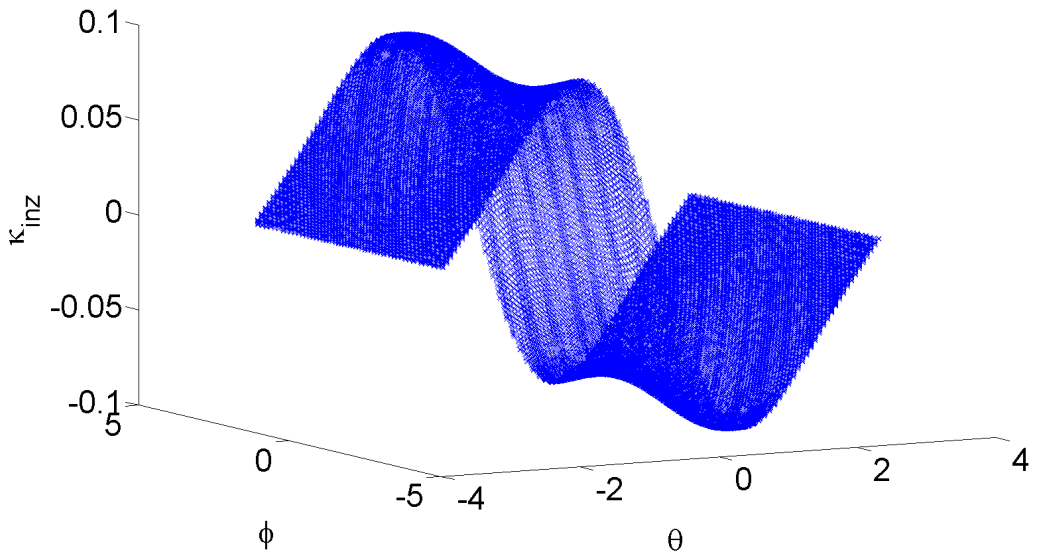

Figure 27: z component of the field-line curvature vector $\boldsymbol{\kappa}$ at the inner interface for a deformation $R_{01} = -Z_{01} = 3 \cdot 10^{-3}$, $R_{21} = Z_{21} = 3 \cdot 10^{-3}$ to a torus of toroidal radius 1.0 and of poloidal radius 0.2

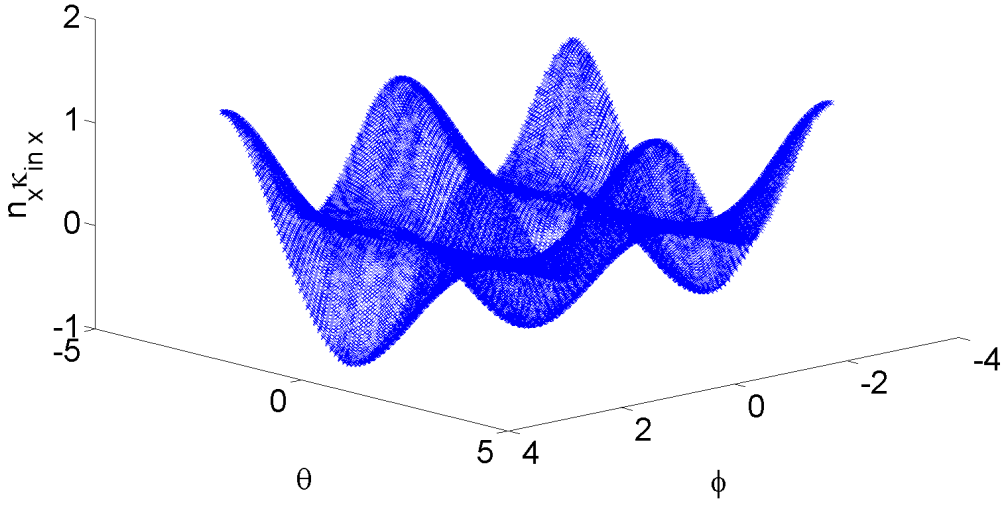

Figure 28: $n_x \kappa_x$ at the inner interface for a deformation $R_{01} = -Z_{01} = 3 \cdot 10^{-3}$, $R_{21} = Z_{21} = 3 \cdot 10^{-3}$ to a torus of toroidal radius 1.0 and of poloidal radius 0.2

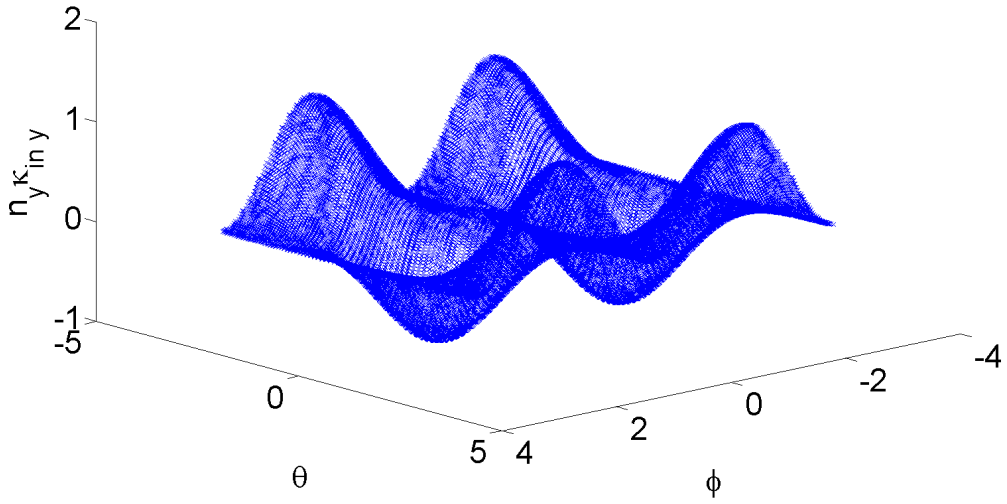

Figure 29: $n_y\kappa_y$ at the inner interface for a deformation $R_{01} = -Z_{01} = 3 \cdot 10^{-3}$, $R_{21} = Z_{21} = 3 \cdot 10^{-3}$ to a torus of toroidal radius 1.0 and of poloidal radius 0.2

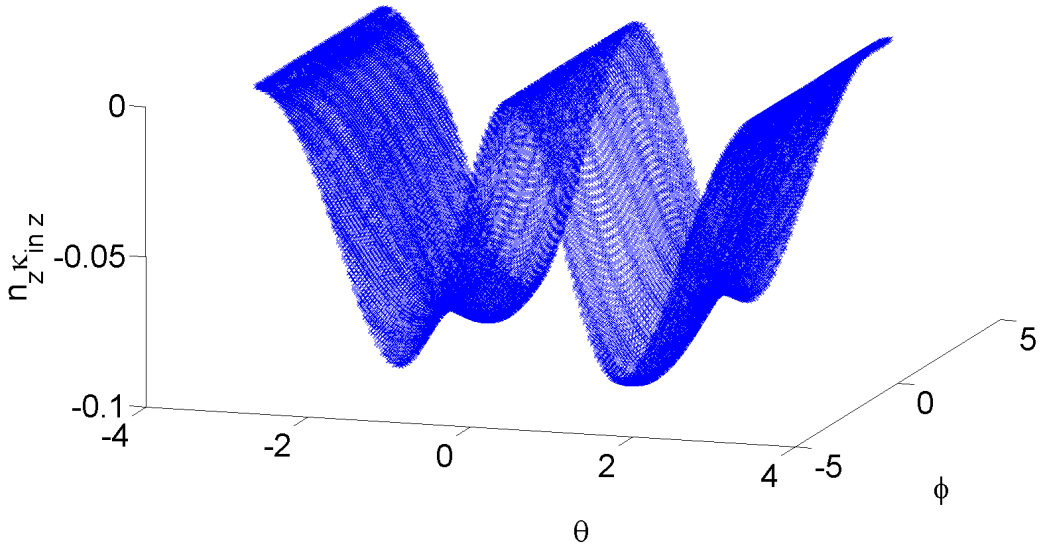

Figure 30: $n_z\kappa_z$ at the inner interface for a deformation $R_{01} = -Z_{01} = 3 \cdot 10^{-3}$, $R_{21} = Z_{21} = 3 \cdot 10^{-3}$ to a torus of toroidal radius 1.0 and of poloidal radius 0.2

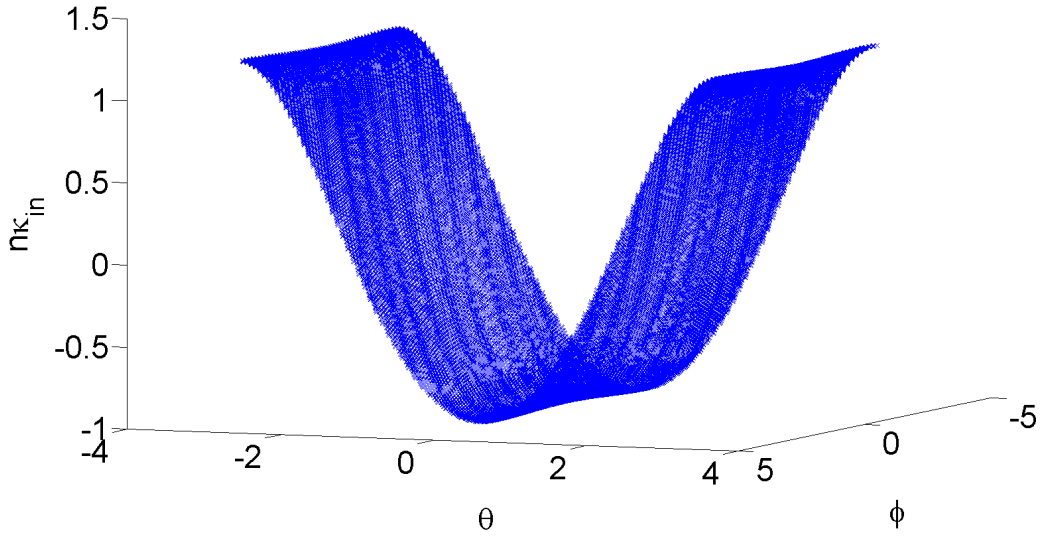

Figure 31: $\boldsymbol{n} \cdot \boldsymbol{\kappa}$ at the inner interface for a deformation $R_{01} = -Z_{01} = 3 \cdot 10^{-3}$, $R_{21} = Z_{21} = 3 \cdot 10^{-3}$ to a torus of toroidal radius 1.0 and of poloidal radius 0.2

7.7. Displacement of the interface, perturbation from equilibrium

To compute the energy variation, we had to specify the displacement $\boldsymbol{\xi}$ (see equation 22) on the interface. We choose a displacement $\boldsymbol{\xi}^{\pm} = \xi_0 \boldsymbol{f}^{\pm}(x,y) e^{iS(\theta,\zeta,s)/\epsilon + i\omega t}$ such that $\boldsymbol{f}^{\pm}(x,y)$ satisfies equation 127. Thus, we are looking for an expression of the form

$$\begin{pmatrix} f_\theta^{\pm} \\ f_\zeta^{\pm} \\ f_s^{\pm} \end{pmatrix} = \begin{pmatrix} \mp i k_\theta \\ \mp i k_\zeta \\ \sqrt{k_\theta k_\theta g^{\theta\theta} + 2 k_\theta k_\zeta g^{\theta\zeta} + k_\zeta k_\zeta g^{\zeta\zeta}} \end{pmatrix} h^{\pm}(\theta,\zeta) \tag{225}$$

Further, we want to consider a displacement which is local, i.e. which goes to zero very fast as we go away from (θ_0, ζ_0). We thus choose the h function such that

$$h^{\pm}(\theta,\zeta) = e^{-C_\theta |\theta-\theta_0| g^{\theta\theta} - C_\zeta |\zeta-\zeta_0| g^{\zeta\zeta}} \tag{226}$$

where $C_\theta << \frac{\max(\|k_\theta\|, \|k_\zeta\|)}{\epsilon}$ and $C_\zeta << \frac{max(\|k_\theta\|, \|k_\zeta\|)}{\epsilon}$. Which leads to the following expression for the displacement:

$$\begin{pmatrix} \xi_\theta^{\pm} \\ \xi_\zeta^{\pm} \\ \xi_n^{\pm} \end{pmatrix} = \xi_0 \begin{pmatrix} \mp i k_\theta \\ \mp i k_\zeta \\ \sqrt{k_\theta k_\theta g^{\theta\theta} + 2 k_\theta k_\zeta g^{\theta\zeta} + k_\zeta k_\zeta g^{\zeta\zeta}} \end{pmatrix}$$

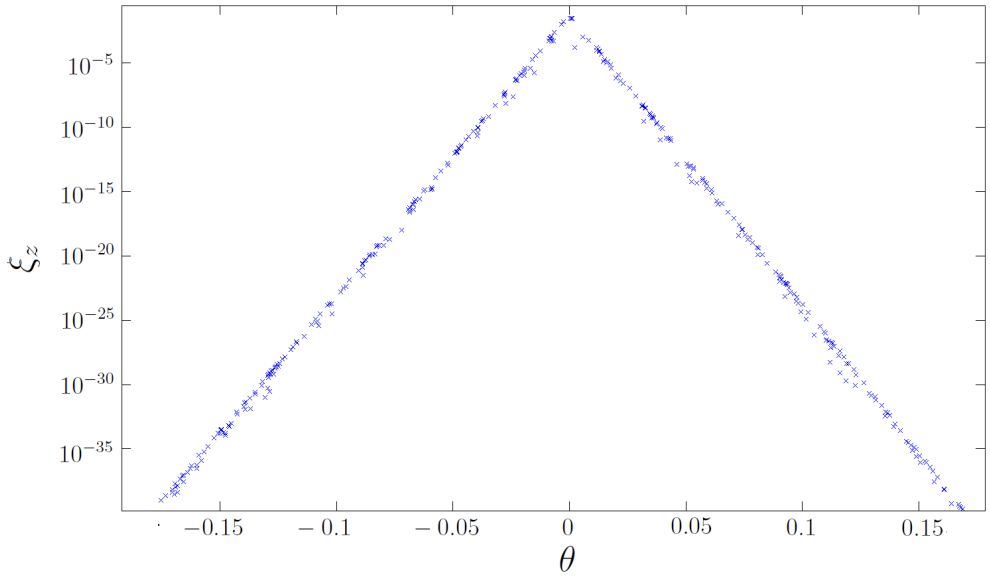

Figure 32: $\|\xi_z\|$ as a function of θ. We see that the displacement is very local.

$$\cdot \exp(ik_\theta|\theta-\theta_0|g^{\theta\theta}+ik_\zeta|\zeta-\zeta_0|g^{\zeta\zeta}\mp ik_s|s-s_0|g^{ss})$$
$$\cdot \exp(-C_\theta|\theta-\theta_0|g^{\theta\theta}-C_\zeta|\zeta-\zeta_0|g^{\zeta\zeta}) \quad (227)$$

Figure 32 shows the normal component of the displacement as a function of θ, for 4 different ζ values. We see that the displacement decreases very fast as we go away from $\theta_0 = 0$. This decrease is due to the term $\exp(-C_\theta|\theta-\theta_0|g^{\theta\theta}-C_\zeta|\zeta-\zeta_0|g^{\zeta\zeta})$. A zoom on a very small θ range shows the oscillation induced by the $\exp(ik_\theta|\theta-\theta_0|g^{\theta\theta}+ik_\zeta|\zeta-\zeta_0|g^{\zeta\zeta}\mp ik_s|s-s_0|g^{ss})$ term.

7.8. Study of the dominant terms in the magnetic field variation $\boldsymbol{b}$

Let us now study the first term of the $\delta^2 W$ expression 148

$$\int_i d^2\sigma \left[\!\left[\xi_0^2(\boldsymbol{n}\cdot\boldsymbol{f}^*)\boldsymbol{B}\cdot\boldsymbol{b}\right]\!\right] \quad (228)$$
$$(229)$$

and in particular, let us focus on the $\boldsymbol{b}$ components. We will here only consider the outside magnetic field perturbation θ component. The same analysis can be made for the ζ component and for the inner field perturbation. b_θ is given by the sum of 12 terms:

$$b_\theta^\pm = \sum_{i=1,12} t_i^\pm \frac{g_{\theta\theta}}{g} \quad (230)$$

where

$$t_1^{\pm} = -\frac{d\xi_s^{\pm}}{ds} B_\theta^{\pm} g_{\zeta\zeta} \tag{231}$$

$$t_2^{\pm} = -\xi_s^{\pm} \frac{dB_\theta^{\pm}}{ds} g_{\zeta\zeta} \tag{232}$$

$$t_3^{\pm} = -\xi_s^{\pm} B_\theta^{\pm} ds \frac{dg_{\zeta\zeta}}{ds} \tag{233}$$

$$t_4^{\pm} = \frac{d\xi_\theta^{\pm}}{d\zeta} B_\zeta^{\pm} g_{ss} \tag{234}$$

$$t_5^{\pm} = -\frac{d\xi_\zeta^{\pm}}{d\zeta} B_\theta^{\pm} g_{ss} \tag{235}$$

$$t_6^{\pm} = \xi_\theta^{\pm} \frac{dB_\zeta^{\pm}}{d\zeta} g_{\zeta\zeta} \tag{236}$$

$$t_7^{\pm} = -\xi_\zeta^{\pm} \frac{dB_\theta^{\pm}}{d\zeta} g_{\zeta\zeta} \tag{237}$$

$$t_8^{\pm} = \xi_\theta^{\pm} B_\zeta^{\pm} \frac{dg_{ss}}{d\zeta} \tag{238}$$

$$t_9^{\pm} = -\xi_\zeta^{\pm} B_\theta^{\pm} \frac{dg_{ss}}{d\zeta} \tag{239}$$

$$t_{10}^{\pm} = -\frac{1}{2g} \xi_\theta^{\pm} B_\zeta^{\pm} g_{ss} \frac{dg}{d\zeta} \tag{240}$$

$$t_{11}^{\pm} = \frac{1}{2g} \xi_\zeta^{\pm} B_\theta^{\pm} g_{ss} \frac{dg}{d\zeta} \tag{241}$$

$$t_{12}^{\pm} = \frac{1}{2g} \xi_s^{\pm} B_\theta^{\pm} g_{\zeta\zeta} \frac{dg}{ds} \tag{242}$$

We first consider an interface which is a perfectly axisymmetric torus. Note that in this specific case, the terms t_6, t_7, t_8, t_9, t_{10} and t_{11} vanish since the interface is symmetric in ζ. Here t_2 is also equal to zero, for reasons explained further on in this paper. Figure 33 shows the amplitude of the 5 different other terms. We see, as expected, that the terms implying a derivative of $\boldsymbol{\xi}$ are the 3 dominant ones. Note that every time we are plotting results in a semi-logarithmic scale, we have taken the absolute value of the terms. Now, if we study the impact of the 3 dominating terms around the zero magnetic shear point, we see that the sum of t_1, t_4 and t_5 goes to zero when we come close to zero magnetic shear (figure 34). In that case, the $\boldsymbol{b}_\theta$ expression is dominated by the t_{12} and t_3 terms. Note that these 2 terms are the one implying derivatives of the metric in the normal direction. We recall here an important assumption we have made before. To obtain the covariant basis vector, we needed to define the derivative of R_{mn} and Z_{mn} with respect to s. We decided to take $\partial R_{mn}/\partial s = C_{mn}$ and $\partial Z_{mn}/\partial s = D_{mn}$, where the C_{mn} and D_{mn} are constants,

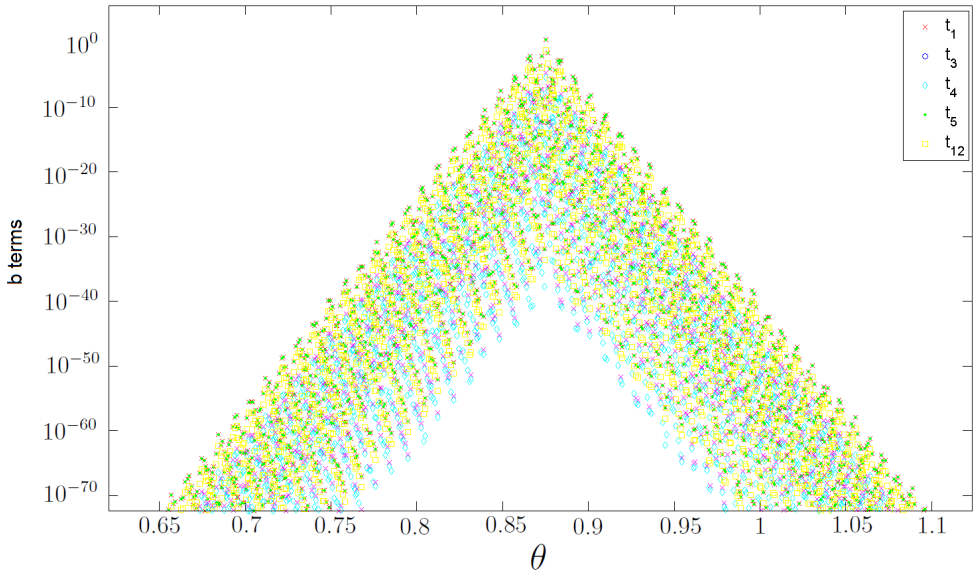

Figure 33: Amplitude of the different terms in the $\boldsymbol{b}$ expression, in the case of a toroidal perfectly axisymmetric surface

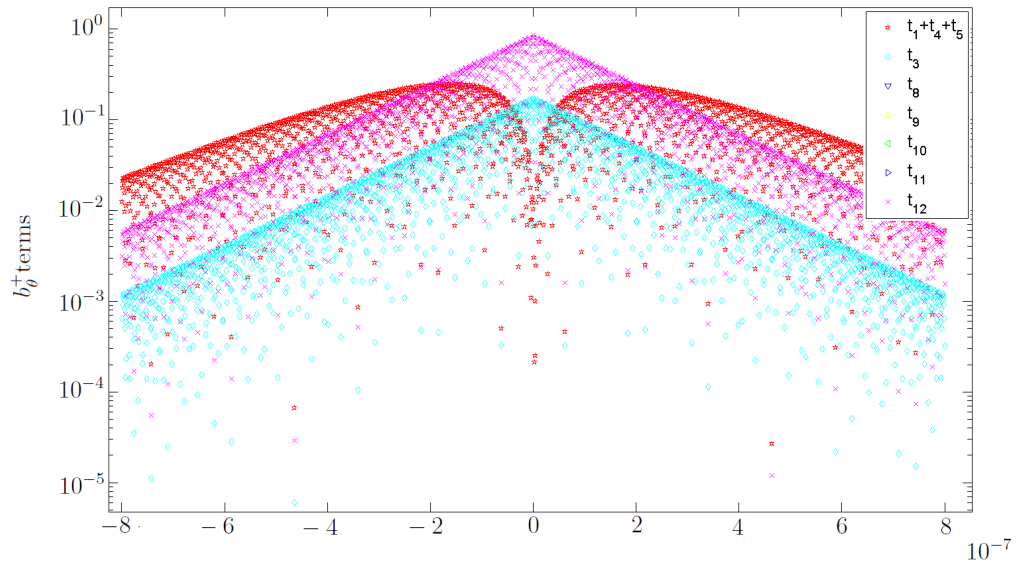

Figure 34: Amplitude of the different terms in the $\boldsymbol{b}$ expression, in the case of a toroidal perfectly axisymmetric surface, for a displacement ξ applied to a point close to zero magnetic shear

because we expected the interface deformation to grow linearly while increasing the radius. If, in contrast, we simply make the assumption that the metric is constant as s increases, i.e. that $\partial R_{mn}/\partial s = \partial Z_{mn}/\partial s = 0$, the terms t_3 and t_{12} cancel out, and we are left only with the terms implying derivatives in ξ, whose sum goes to zero when we approach the point of zero magnetic shear.

Another hypothesis we had to make was to define the variation of the magnetic potential $f^{\pm}$ as a function of s. We recall here that

$$f^{\pm} = C^{\pm}_{\Theta}\Theta + C^{\pm}_{z} Z + \sum f^{\pm}_{mn} \sin(m\theta - n\zeta) \tag{243}$$

where C_Θ and C_z are constants. As the pressure is constant within a definite plasma volume, we made the hypothesis that $\partial f^{\pm}_{mn}/\partial s = 0$ inside a plasma region. Thus $\partial \boldsymbol{B}^{\pm}/\partial s = 0$. That is why the term $t_2 = 0$.

If we apply a deformation, we get results close to the one obtained for an axisymmetric toroidal surface. Note that if we consider a deformed interface, the terms t_6, t_7, t_8, t_9, t_{10} and t_{11} are no longer equal to zero. But, if we consider a deformation as defined in 227, we realize that the contribution of these 6 terms is purely imaginary at the point of zero magnetic shear where the displacement $\boldsymbol{\xi}$ is applied. We are then left just with a situation where we need to compare the impact of the 3 terms involving the ξ derivatives, the terms t_3 and t_{12} and the curvature term.

7.9. Dominant terms in the $\delta^2 W$ expression for points close to zero magnetic shear

Figure 35 shows the contributions of all the terms for a perfectly axisymmetric torus, in the case where the outside pressure is equal to the inner one diminished by 30%, and when the displacement is extremely local. We see that the 3 terms involving the ξ derivatives dominate generally, but that when we come close to zero magnetic shear, the sign of the $\delta^2 W$ expression is given by the curvature term. The impact of the t_3 and t_{12} terms is smaller than the curvature term. Figure 36 shows a zoom for a region close to zero magnetic shear. Let us now study how close to the point of zero magnetic shear, the curvature term starts being dominant. Figure 37 shows for which $\delta\theta = \theta - \theta_{\text{minshear}}$ the curvature term start dominating, for different K values, where K is defined through the k_θ and k_ζ expressions (taking $\epsilon = 1$):

$$k_\theta = (B_\zeta g^{\zeta\zeta} + B_\theta g^{\theta\zeta})K \tag{244}$$

$$k_\zeta = (B_\theta g^{\theta\theta} + B_\theta g^{\theta\zeta})K \tag{245}$$

On figure 37, we see that, the bigger the K value, the closer we need to go to the zero shear point to have the curvature term dominating. The relation between $\delta\theta$ and K is a straight line in a log/log scale. We can thus say that the system is more stable for bigger K. Figure 38 shows the same relation between $\delta\theta$ and K,

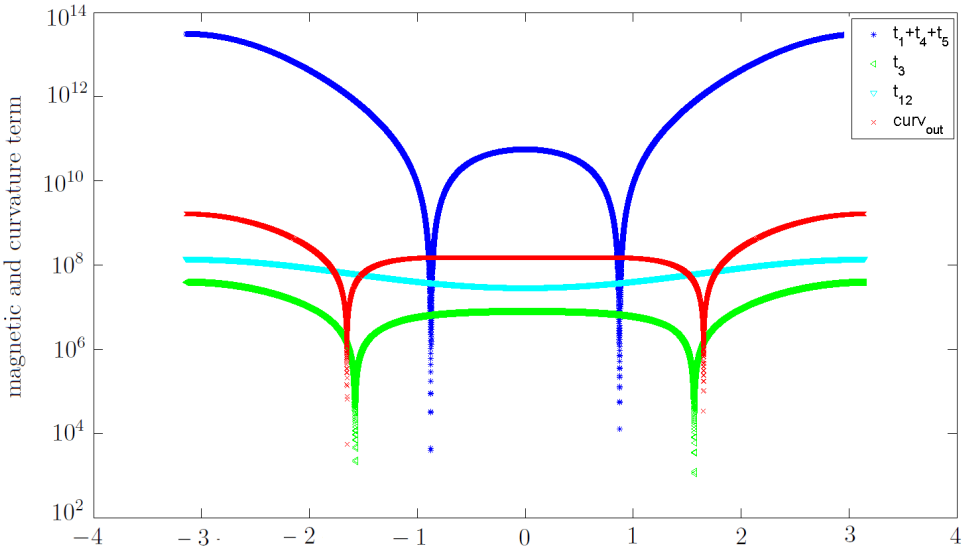

Figure 35: Magnetic and curvature terms in the second energy variation expression, in the case of a toroidal perfectly axisymmetric surface

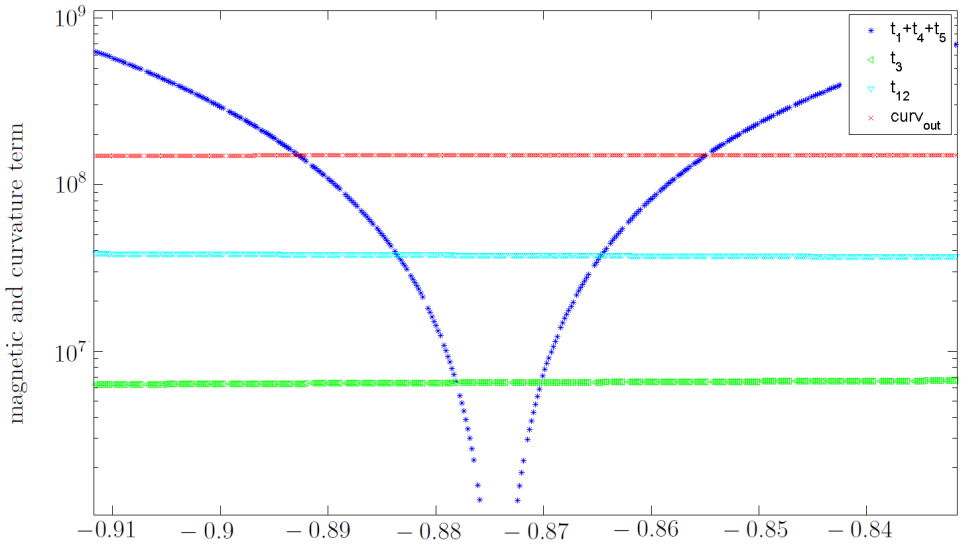

Figure 36: Magnetic and curvature terms in the second energy variation epxression, in the case of a toroidal perfectly axisymmetric surface, for points close to zero magnetic shear

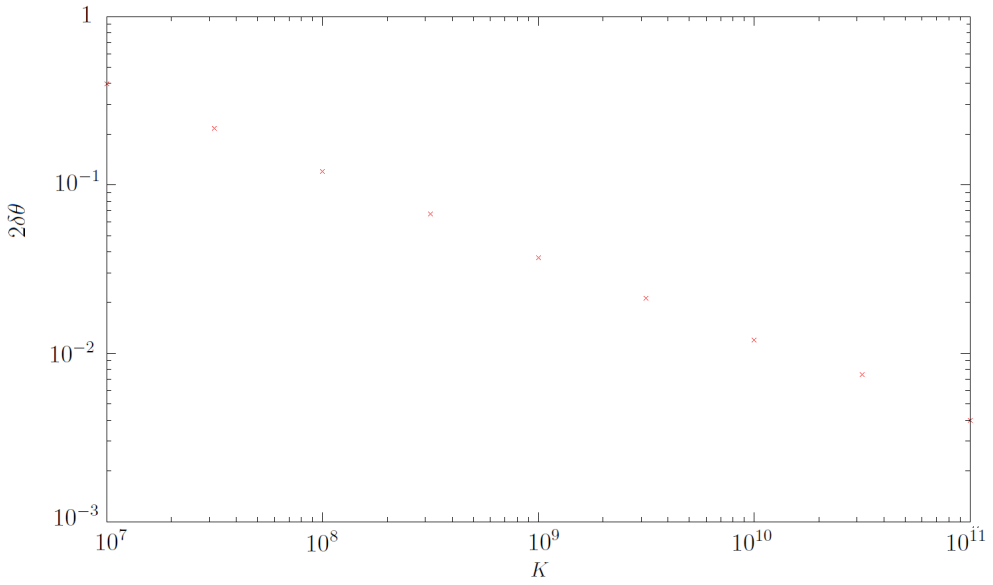

Figure 37: θ value at which the curvature term starts dominating over the magnetic term, for different K values, in the case where the interface is a perfectly axisymmetric torus

in the case where the surface is a deformed torus with $R_{01} = -Z_{01} = 0.7 \cdot 10^{-2}$, $R_{21} = Z_{21} = 0.7 \cdot 10^{-2}$. The toroidal radius is given by $R_0 = 1.0$ and the poloidal radius $R_1 = 0.2$. We see again that the relation between $\delta\theta$ and K is a straight line if we use a log/log scale. $\delta\theta$ decreases from a factor 10 when K increases from a factor 10^2. Further, we note that for a given K, we need to go much closer to the point of zero magnetic shear than in the case when the interface is a perfectly axisymmetric torus, to have to curvature term dominating. Thus, the stability of the interface, close to zero magnetic shear, depends both on the shape of the interface and on the amplitude of the displacement derivatives.

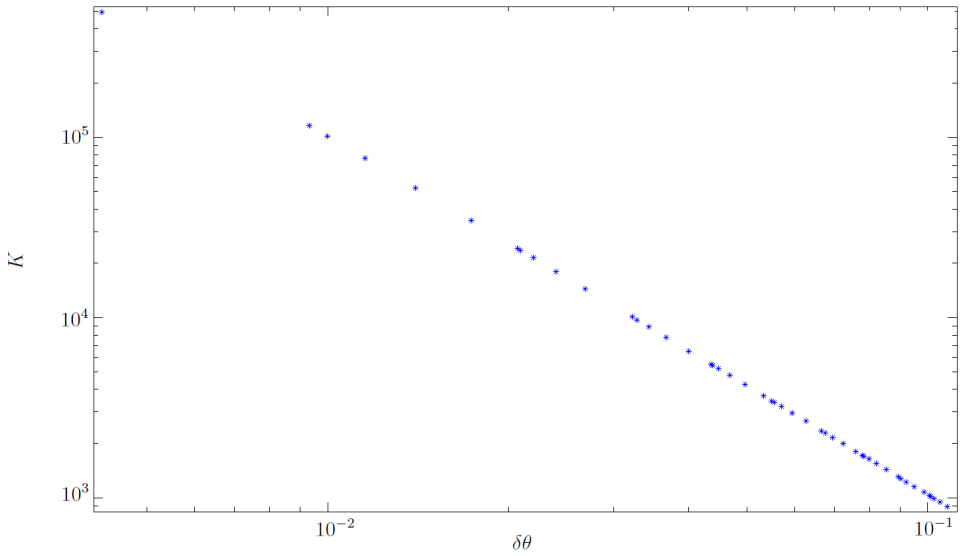

Figure 38: θ value at which the curvature term starts dominating over the magnetic term, for different K values when the interface is a deformed torus with $R_{01} = -Z_{01} = 0.7 \cdot 10^{-2}$, $R_{21} = Z_{21} = 0.7 \cdot 10^{-2}$ and with $R_0 = 1.0$ and $R_1 = 0.2$.

7.10. Stability and pressure jump

We finally study the impact of the pressure jump on the stability. We consider an interface with $R_{01} = -Z_{01} = 0.5 \cdot 10^{-2}$, $R_{21} = Z_{21} = 0.5 \cdot 10^{-2}$ and with $R_0 = 1.0$ and $R_1 = 0.2$. Figure 39 shows for which θ values the system starts being unstable for different pressure variations at the interface. We see that the bigger the pressure jump (on the figure, -100% signify that the outside field is zero while 0% means that the outer field is equal to the inner one), the more unstable the plasma is. This is true because we consider points located away from the vertical axis of the torus. If we were studying points closer to the central axis where the curvature term is stabilizing, the conclusion would be the opposite. Note that the discrete points relating Δp to the θ values at wich the system starts being unstable are pretty well fitted by a second degree equation. This might be due to the fact that Δp is proportional to $[\![B^2]\!]$.

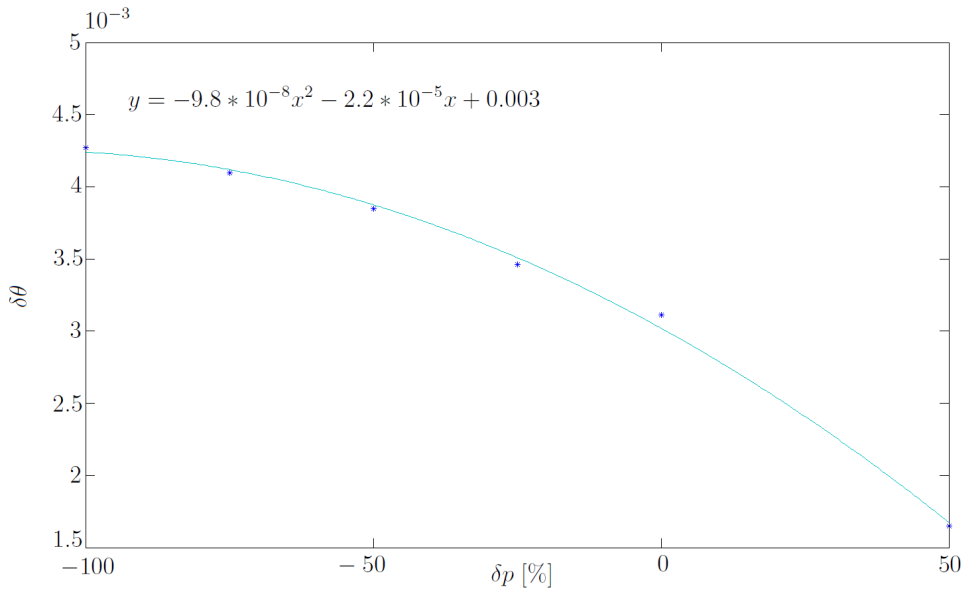

Figure 39: θ value at which the curvature term starts dominating over the magnetic term, for different pressure variations Δp, when the interface is a deformed torus with $R_{01} = -Z_{01} = 0.5 \cdot 10^{-2}$, $R_{21} = Z_{21} = 0.5 \cdot 10^{-2}$ and with $R_0 = 1.0$ and $R_1 = 0.2$.

8. Conclusion

The study presented in this paper is part of a more general project on constructing 3-D MHD equilibria, in a way fully compatible with the existence of chaotic magnetic fields. One crucial point in this model is establishing the existence and stability of good magnetic surfaces with irrational rotational transform that can sustain a pressure jump. Though the existence of surfaces that satisfy force balance is quite well established [2], the question of stability to displacements of the interface still had to be investigated. In this study, we adapted a theory developed by Bernstein *et al* [4] for high-n MHD stability at an interface between a vacuum magnetic field and a field-free plasma to the problem of general fields. We computed the second energy variation for a plasma interface at equilibrium and showed that the equilibrium was stable to displacements localized about most points on the surface. We then focused on the stability at an interface for points close to zero magnetic shear, where the magnetic term and the curvature term start competing. Only at this kind of points can the equilibrium become unstable. We found a simple sufficient condition for high-n interface stability to surface displacement: the interface is stable if all points of zero magnetic shear have favorable curvature.

We implemented the theoretical results on a test case by modifying McGann's PJH code. We showed the influence of the different terms in the energy variation equation and studied when the curvature term starts dominating over the term due to the magnetic field variation. We showed that the system was more stable when the displacement derivatives were big and gave a relation between these derivatives and the point at which the second variation of the energy starts being negative. We thus got a better understanding of the stability to displacements of a plasma interface.

This multiple relaxation region MHD model raises a number of questions and there are a few subjects related to this work that should be further investigated. One example on which research has been done recently is the study of the maximum pressure jump an interface can support before being destroyed by instabilities and chaos. Another field of investigation, suggested by Hole [30], is to explore the use of the double Beltrami model [18]. This model has been shown to be useful for describing the phenomenology of the pressure pedestal in H-mode tokamak discharge [19]. It is also needed to push this research further to find an analytic stability criterion in cases where zero shear points have unfavorable curvature.

9. Acknowledgement

This research was performed at ANU with support from the Research School of Physics and Engineering and the PTM group. The author would like to thank in particular Prof. Robert L. Dewar and Dr. Matthew J. Hole for their valuable remarks, discussions and comments and Mathew McGann for providing him with the PJH code. Part of this research was undertaken on the NCI National Supercomputing Facility in Canberra, Australia, which is supported by the Australian Commonwealth Government. The Author also thanks EPFL for its financial support.

References

[1] Dewar R L *et al* 2008 *Entropy* **10** 621-634
[2] McGann M, Hudson S R Dewar R L and von Nessi G 2010 *Physics Letters A* **374** 33083314
[3] Cuthbert P and Dewar R L 2000 *Phys. Plasmas* **7** 2302
[4] Bernstein I B, Frieman E A, Kruskal M D and Kulsrud R M 1958 *Proc. R. Soc. London* Ser. A **244** 17
[5] Spies G O 2003 *Physics of Plasmas* **10** (7) 3030-3031
[6] Mills R L, Hole M J and Dewar R L 2009 *Plasma Physics* **75** (5) 637659
[7] Hole M J, Hudson S R and Dewar R L 2007 *Nuclear Fusion* **47** (5) 746753
[8] Dewar R L *et al* , *Variational principle for multi-region three-dimensional relaxed magnetohydrodynamic equilibria* (unpublished)
[9] Boozer A H 2004 *Rev. Mod. Phys.* **44** 10711138
[10] Grad H 1967 *Phys. Fluids* **10** 137154
[11] Lichtenberg A J and Lieberman M A 1992 *Regular and Chaotic Dynamics.* NewYork: Springer
[12] Taylor J B 1986 *Rev. Mod. Phys.* **58** 741
[13] Kaiser R and Uecker H 2004 *Q. J. Mech. Appl. Math. 57* 117
[14] Newcomb W A 1960 *Ann. Phys. 10* 232267
[15] Edenstrasser J W 1988 *Plasma Physics and Controlled Nuclear Fusion Research* Proceedings of the Twelth Conference, Nice
[16] Spies G O, Lortz D and Kaiser R 2001 *Physics of Plasmas* **b** 3652-3663
[17] Hole M J, Hudson S R, Dewar R L 2006 *J. Plasma Physics* **72** 1167-1171
[18] Yoshida Z and Mahajan S M 2002 *Phys. Rev. Lett.* **88** 095001
[19] Guzdar P N, Mahajan S M and Yoshida Z 2005 *Phys. Plasmas* **12** 032502
[20] Taylor J B 1974 *Phys. Rev. Letters* **33** 1139-1141
[21] Dewar R L 1997 *Journal of Plasma and Fusion Research* **73** 1123-1134
[22] McMillan B F, Dewar R L and Storer R G 2004 *PPCF* **46** 1027-1038
[23] Kress R 1986 *JEM* **20** 323-344
[24] Kress R 1981 *JEM* **15** 29-48
[25] Colton D, Kress R 1983 *Integral equation methods in scattering theory* New York: J. Wiley
[26] Moroz P E 1998 *Physics Letters A* **243** 60-65
[27] Kuo-Petravic G and Boozer A H 1987 *Journal of Computational Physics* **73** 107-124
[28] Percival I C 1974 *J. Phys. A* **7** 794
[29] Sunn Pedersen T and Boozer A H 2002 *Phys. Rev. Letters* **88** 205002
[30] Hole M J, Mills R, Hudson S R and Dewar R L 2009 *Nuclear Fusion* **49** 065019
[31] Hirshman S P and Whitson 1983 Phys Fluid 26 3553
[32] Reiman H and Greenside H S 1988 J Comput Phys 75 423
[33] Gardner J and Blackwell B 1992 Nucl Fusion 32 2009
[34] Hudson S R, Hole M J and Dewar R L 2007 Phys Plasmas 14 052505
[35] Hole M J, Hudson S R, Dewar R L, McGann M and Mills R *Relaxed MHD states of a multiple region plasma*, poster
[36] http://www.cea.fr/energie/fusion_controlee_la_terre_sur_les_traces_du_so/le_tokamak_du_plasma_en_boite (31.09.2010)
[37] http://www.efda.org/fusion_energy/fusion_as_an_energy_source.htm (31.09.2010)
[38] wikipedia.org
[39] R L Dewar, *MHD Lagrangian and ballooning modes*, Power point presentation

10. Annexes

10.1. field-line curvature vector

Let us prove that the field-line curvature vector is perpendicular to the magnetic field. We use the gradient identity

$$\boldsymbol{B}\cdot\boldsymbol{\nabla}\boldsymbol{B}=\boldsymbol{\nabla}\frac{B^2}{2} \tag{246}$$

And rewrite it using 146

$$B\boldsymbol{e}_{\parallel}\cdot\boldsymbol{\nabla}\boldsymbol{B}\boldsymbol{e}_{\parallel}=\boldsymbol{\nabla}\frac{B^2}{2} \tag{247}$$

$$B^2\boldsymbol{\kappa}+\boldsymbol{e}_{\parallel}\cdot(\boldsymbol{\nabla}\frac{B^2}{2})\boldsymbol{e}_{\parallel}=\boldsymbol{\nabla}\frac{B^2}{2} \tag{248}$$

$$B^2\boldsymbol{\kappa}=(\boldsymbol{I}-\boldsymbol{e}_{\parallel}\boldsymbol{e}_{\parallel})\cdot\boldsymbol{\nabla}\frac{B^2}{2} \tag{249}$$

And finally

$$\boldsymbol{\kappa}=\frac{1}{B^2}\cdot\boldsymbol{\nabla}_{\perp}\frac{B^2}{2} \tag{250}$$

which proves that $\boldsymbol{\kappa}\cdot\boldsymbol{B}=0$.

10.2. Green functions, detailed calculus

Let start from the expression of $\boldsymbol{b}$

$$\begin{aligned}\boldsymbol{b}(\boldsymbol{r})=&-(\boldsymbol{\nabla}\times+\mu)\int_S\Phi(\boldsymbol{r},\boldsymbol{r'})(\boldsymbol{n}(\boldsymbol{r'})\times\boldsymbol{b}(\boldsymbol{r'}))dS(\boldsymbol{r'})\\&-\boldsymbol{\nabla}\int_S\Phi(\boldsymbol{r},\boldsymbol{r'})\{\boldsymbol{B}(\boldsymbol{r'})\cdot\boldsymbol{\nabla}\xi(\boldsymbol{r'})\\&+\xi(\boldsymbol{r'})\boldsymbol{n}(\boldsymbol{r'})\cdot\boldsymbol{\nabla}\times[\boldsymbol{n}(\boldsymbol{r'})\times\boldsymbol{B}(\boldsymbol{r'})]\}dS(\boldsymbol{r'})\end{aligned} \tag{251}$$

and consider the Fourier transform of $\boldsymbol{b}$

$$\boldsymbol{b}(\boldsymbol{r})=\int\boldsymbol{b}_k e^{i\boldsymbol{k}\cdot\boldsymbol{r}}dk^3 \tag{252}$$

and of ξ

$$\xi(\boldsymbol{r})=\int\xi_k e^{i\boldsymbol{k}\cdot\boldsymbol{r}}dk^3 \tag{253}$$

We also use the particular solution to the Helmoltz equation

$$\Phi_1(\boldsymbol{r},\boldsymbol{r'})=\frac{-i\mu}{4\pi^2}\int d^3k\frac{e^{i\boldsymbol{k}\cdot(\boldsymbol{r}-\boldsymbol{r'})}}{k^2-\mu^2} \tag{254}$$

Inserting 252, 253 into 251 and using the Fourier form of the Green function 254, we get

$$\begin{aligned}\int \boldsymbol{b}_k e^{i\boldsymbol{k}\cdot\boldsymbol{r}} dk^3 = & -(\boldsymbol{\nabla}\times+\mu)\int dk^3 \int_S \frac{1}{4\pi^2}\int d^3k' \frac{e^{i\boldsymbol{k'}(\boldsymbol{r}-\boldsymbol{r'})}}{k'^2-\mu^2} \\ & (\boldsymbol{n}(\boldsymbol{r'})(\boldsymbol{r'})\times \boldsymbol{b}_k e^{i\boldsymbol{k}\boldsymbol{r'}})dS' \\ & + \boldsymbol{\nabla}\int_S \frac{i\mu}{4\pi^2}\int d^3k' \frac{e^{i\boldsymbol{k'}(\boldsymbol{r}-\boldsymbol{r'})}}{k'^2-\mu^2}\int dk^3\{\boldsymbol{B}(\boldsymbol{r'})\cdot\boldsymbol{\nabla}\xi_k e^{i\boldsymbol{k}\cdot\boldsymbol{r'}} \\ & + \xi_k e^{i\boldsymbol{k}\cdot\boldsymbol{r'}}\boldsymbol{n}(\boldsymbol{r'})\cdot\boldsymbol{\nabla}\times[\boldsymbol{n}(\boldsymbol{r'})\times\boldsymbol{B}(\boldsymbol{r'})]\}dS' \end{aligned} \tag{255}$$

We then rearrange the terms to isolate the surface integral

$$\begin{aligned}\int \boldsymbol{b}_k e^{i\boldsymbol{k}\cdot\boldsymbol{r}} dk^3 = & -\frac{1}{4\pi^2}(\boldsymbol{\nabla}\times-\mu)\int dk^3\int d^3k'\frac{1}{k'^2-\mu^2} \\ & \cdot(\boldsymbol{n}(\boldsymbol{r'})\times\boldsymbol{b}_k)e^{i\boldsymbol{k'}\boldsymbol{r}}\int_S e^{i(\boldsymbol{k}\cdot\boldsymbol{r'}-\boldsymbol{k'}\boldsymbol{r'})}dS' \\ & + \boldsymbol{\nabla}\frac{i\mu}{4\pi^2}\int d^3k'\int dk^3\frac{1}{k'^2-\mu^2}[i\boldsymbol{B}\cdot\boldsymbol{k}\xi_k \\ & + \xi_k\boldsymbol{n}\cdot\boldsymbol{\nabla}\times(\boldsymbol{n}\times\boldsymbol{B})]e^{i\boldsymbol{k'}\boldsymbol{r}}\int_S e^{i(\boldsymbol{k}\cdot\boldsymbol{r'}-\boldsymbol{k'}\boldsymbol{r'})}dS' \end{aligned} \tag{256}$$

We notice that the surface integral is nothing but the definition of the delta function to within a factor.

$$\int_S e^{i(\boldsymbol{k}\cdot\boldsymbol{r'}-\boldsymbol{k'}\boldsymbol{r'})}dS' = \delta(\boldsymbol{k}-\boldsymbol{k'}) \tag{257}$$

Thus, replacing 257 in 256, we finally get

$$\begin{aligned}&\int \boldsymbol{b}_k e^{i\boldsymbol{k}\cdot\boldsymbol{r}}d\boldsymbol{k} + \frac{1}{4\pi^2}(\boldsymbol{\nabla}\times+\mu)\int d^3k\frac{1}{k^2-\mu^2}(\boldsymbol{n}\times\boldsymbol{b}_k)e^{i\boldsymbol{k}\cdot\boldsymbol{r}} \\ &= \boldsymbol{\nabla}\frac{i\mu}{4\pi^2}\int d^3k\frac{1}{k^2-\mu^2}[i\boldsymbol{B}\cdot\boldsymbol{k}\xi_k \\ &+\xi_k\boldsymbol{n}\cdot\boldsymbol{\nabla}\times(\boldsymbol{n}\times\boldsymbol{B})]e^{i\boldsymbol{k}\cdot\boldsymbol{r}} \end{aligned} \tag{258}$$

We thus find an expression relating $\boldsymbol{b}_k$ to $\boldsymbol{B}$ and ξ_k which can be further developped by expanding $\boldsymbol{B}$ about a line of zero shear